ADVANCED PHYSICS RESEARCH Open Access
www.advphysicsres.com

Bioelectronics with Topological Crosslinked Networks for Tactile Perception

*Mingqi Ding, Pengshan Xie, and Johnny C. Ho**

Bioelectronics, which integrate biological systems with electronic components, have attracted significant attention in developing biomimetic materials and advanced hardware architectures to enable novel information-processing systems, sensors, and actuators. However, the rigidity of conjugated molecular systems and the lack of reconfigurability in static crosslinked structures pose significant challenges for flexible sensing applications. Topological crosslinked networks (TCNs) featuring dynamic molecular interactions offer enhanced molecular flexibility and environmentally induced reconfigurability, decoupling the competition between performances. Here, recent advances are summarized in assembly methods of bioelectronics with different TCNs and elaborate ion/electron-transport mechanisms from the perspective of molecular interactions. Decoupling effects can be achieved by comparing distinct TCNs and their respective properties, and an outlook is provided on a new range of neuromorphic hardware with biocompatibility, self-healing, self-powered, and multimodal-sensing capabilities. The development of TCN-based bioelectronics can significantly impact the fields of artificial neuromorphic perception devices, networks, and systems.

1. Introduction

To improve efficiency, reduce error rates, support decision-making, and enhance quality of life, there is a growing demand for advanced functionalities in human-machine interactions, which include applications, such as object manipulation, health monitoring, and material identification.[1–3] Owing to the stiffness and brittleness, conventional silicon-based semiconductors are unsuitable for implantation as a tactile sensing accessory.[4] Neuromorphic devices, employing organic conjugated systems capable of generating intelligent responses to environmental variations, have garnered considerable attention in the field of artificial neuromorphic perception,[5–7] while their segmental rigidity and electronic barriers to ion transport result in suboptimal flexibility and sensitivity.[8] Constructing crosslinked networks with ionic components presents a promising solution to conquer the non-flexibility issue, while ion gels remain susceptible to swelling/dehydration when exposed to the environment.[9] Consequently, it is challenging to decouple the competition in flexibility and conductivity for neuromorphic devices and simultaneously suffice the requirements of sensitivity and stability.

Topological crosslinked networks (TCNs) are polymer arrays comprising monomer units organized through highly oriented and reversible non-covalent bonding interactions.[10–12] Understanding the dynamic interactions in TCNs is critical for elucidating the structure-property relationship, particularly between molecular interactions and viscoelasticity.[13–15] Through modulating the viscoelasticity of TCNs by material processing and external stimuli, molecular flexibility and ion transport of TCNs can be adjusted, and the fabricated ion gels with specific TCNs will be applied in line with the material properties (**Figure 1**). Compared to chemically crosslinked structures, TCNs provide abundant dynamic hydrogen bonds, which enable self-healing properties and improved interfacial adhesion in devices.[16–19] Additionally, designing slide-ring structures through host-guest interactions can increase the free volume available for molecular motion, thereby improving the stretchability of the material.[20–23] Furthermore, the metal-ligand assembled branched nanoclusters possess a regular arrangement of the repeated monomers in one polymer chain,[24–28] whose introduction increases hydrogen-bond crosslinking density, which in turn enhances the mechanical strength of the ion gels.[24] Besides, integrating TCNs with conjugated systems can impart quantum effects or chirality to the ion gels, resulting in distinctive physical properties.[15,25] All these TCNs based on molecular structure design are fundamental to developing neuromorphic devices.

M. Ding, P. Xie, J. C. Ho
Department of Materials Science and Engineering
City University of Hong Kong
Kowloon, Hong Kong SAR 999077, China
E-mail: johnnyho@cityu.edu.hk
J. C. Ho
State Key Laboratory of Terahertz and Millimeter Waves
City University of Hong Kong
Hong Kong SAR999077, China
J. C. Ho
Institute for Materials Chemistry and Engineering
Kyushu University
Fukuoka 816-8580, Japan

The ORCID identification number(s) for the author(s) of this article can be found under https://doi.org/10.1002/apxr.202400165

DOI: 10.1002/apxr.202400165

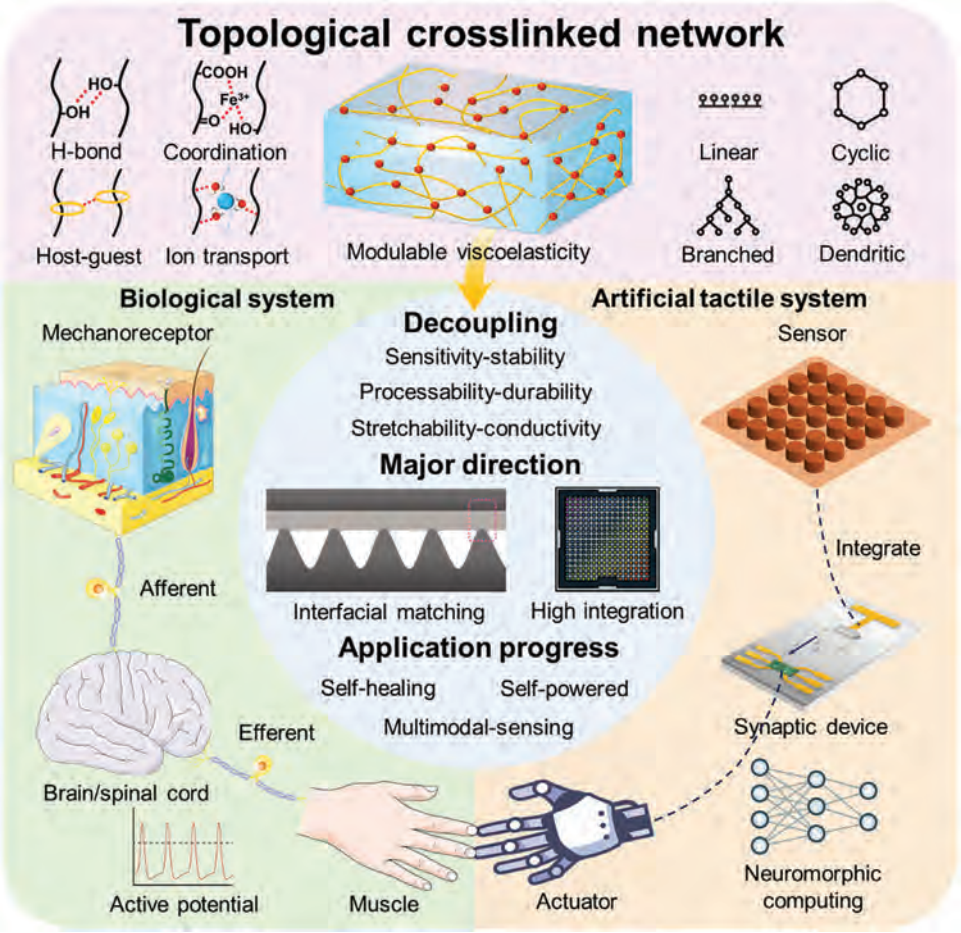

Figure 1. The construction of an artificial tactile system inspired by a biological system. The viscoelasticity can be modulated by rationally designing the molecular configuration/chemical components to decouple the competing effect of device performances.

Bioelectronics is a highly interdisciplinary field, encompassing polymer physics, materials engineering,[26–28] biosensing, integrated circuits, and neuronal algorithms.[29–31] Based on previous research, topological molecular science-guided bioelectronics (TCN-E) have garnered magnificent breakthroughs. Currently, the purpose of topological crosslinking design is to solve three main problems in electronic skin (e-skin) and tactile perception systems (Figure 1): 1) decouple competing effects (i.e., mechanical properties and conductivity) using multiple molecular building blocks to meet complex requirements[32–34]; 2) modulate conductance by molecular reconfiguration (assemble and disassemble) through external-stimuli, enhancing the sensing range of bioelectronic[35–37]; 3) optimize bioelectronic interfaces by combining similar topological molecular systems in conductors, semiconductors, and dielectrics, serving as electrodes, channels and substrates, respectively.[38,39] Besides, the abundant reactive sites and more reconfigurable molecular interactions of TCNs are advantageous in biological sensing and neuromorphic computing, compared with organic electronics of only conjugated semiconducting systems.[40,41] Specifically, biological signals can be transduced into electrical signals through ion-electron coupling for neuromorphic computing.[42–44] Additionally, the reconfigurable molecules in TCN-E endow the capability of modulating synaptic weight.[45,46] Compared with static crosslinked structures, ionic-electronic coupling in TCN-E is efficient owing to unique topology-induced ion transport, such as coordination-assisted single-ion transport in slide-ring structure and proton transport in hydrogen-bonded structure, which in turn improves the sensitivity while processing the afferent biological signals.[47–49] Integrating flexible biosensors with synaptic devices enables perception and computational functions, while the interfacial mechanical mismatch and complexity of the conductance mechanisms remain significant challenges for practical applications.[48,50,51] Consequently, it is crucial to integrate TCN assembly methods with appropriate interaction and conductance modulation mechanisms to rationally design bioelectronics, facilitating the perceptual evolution of neuromorphic devices (Figure 1).

In this review, we discuss recent research wherein bioelectronics are rationally designed by the topological crosslinked structure, the mechanical and physical properties of TCNs with the relative applications of TCN-E. Initially, we systematically summarize the assembly strategy of representative TCNs, which aims at decoupling competition between mechanical and conductive properties, such as dual-network hydrogel, nanocluster-strengthened and slide-ring crosslinked structures, followed by

introducing the basic physical process of organic ionic-electronic conductors and topological structure-induced special conduction mechanism. Afterward, we provide a comprehensive review of recent advances in the design of bioelectronic devices utilizing TCN design for artificial tactile neurons, such as self-powered, self-healable, and multimodal-sensing capabilities. Finally, we investigate handicaps that should be combated to achieve high integration, sensitivity, and stability in the tactile perception system and provide insight into the promising opportunities of TCN-E.

2. Assembly of TCNs

Recently, neuromorphic devices have attracted considerable research interest, with a significant growth in TCN-based ion gels. Notably, according to the distinct molecular interactions, it is stipulated to choose suitable components for assembling different TCNs and achieving relative functions. Structurally, long-chain polymers with plentiful hydroxyl or carboxyl groups are susceptible to forming hydrogen-bonded networks, possessing superior molecular flexibility and biocompatibility.[52] By freeze-thaw cycling and sol-gel transition, dual-network hydrogels possess anti-freezing/anti-swelling and injectability.[53] Additionally, through metal-ligand coordination, nanocluster-strengthened crosslinked networks possess excellent tensile strength due to the increased crosslinking density.[54] In order to optimize engineering technologies, decouple the competing effects, and enhance stretchability, a comprehensive understanding of assembly methods and molecular interactions is prominent. In this chapter, we will introduce the modulation strategy of viscoelasticity by constructing different TCNs and addressing scientific or engineering controversies.

2.1. Dual-Network Hydrogel

A dual-network hydrogel, formed by crosslinking two polymer molecules with hydrogen bonding, possesses enhanced molecular entanglement (**Figure** 2a). Polyvinyl alcohol (PVA), with superior hydrophilicity and biocompatibility, is one of the conventional flexible polymer matrixes for bioelectronics.[55–57] In order to endow PVA-based hydrogels with ionic-electronic conduction capability and mechanical stability, it is necessary to introduce other polymers such as polyacrylamide (PAM), polypyrrole (PPy), polyaniline (PANI), and crosslinking agents into the gel skeleton.[57–60] Besides, the linear and flexible topological nature of PVA endows fast crystallization when complexed with conjugated molecular systems, and the nanocrystals formed by PVA can enhance the interfacial adhesiveness and stability of the hydrogels.[61] Nevertheless, micromolecular crosslinkers will generate dense interaction with the long-chain hydroxyl-full polymers due to the high crosslinking density, hindering the formation of a homogenous molecular structure by mechanical mixing. Notably, the processing temperature is a critical index affecting the strength of hydrogen bonding in molecular networks.[62–64] Detailly, dual-network hydrogels can be synthesized by temperature-triggered sol-gel transition, and freeze-thaw assisted hydrogen reassembly, indicating the processability of bio-engineered integrated circuits (i.e., printing or molding), favorable elasticity, and conductivity. In order to better design the material structure and reaction conditions, the molecular configuration of the polymer and the corresponding molecular weight (MW, unit: g mol^{-1}), viscoelasticity (the ratio of loss and storage modulus, $G''/G' = \tan\delta$), and glass transition temperature (T_g, unit:°C) need to be clarified. The detailed molecular information is illustrated in Figure 2b.

2.1.1. Sol-Gel Transition

Sol-gel transition is a facile assembly method for reconfigurable crosslinked networks, which promises a strategy for circuit painting and injectable printing (Figure 2d).[56,65,66] Modifying water content and viscosity in the system is vital for smooth extrusion. As reported by Niu et al., the flexible and ion-conductive molecular elastomer could be processed by evaporating/casting the aqueous mixture composed of PVA and organic ionic liquid (inositol hexakisphosphate (IP6)).[56] This molecular system is capable of versatile processability, and the fabricated bioelectronics possessed skin-like softness (Young's modulus ≈0.3 MPa), large stretchability (≈573%), and out-standing elastic restorability while displaying excellent ionic conductivity of 4.5×10^{-2} S m^{-1} at 25 °C. However, hydrogen bonding-based hydrogel will become solid-state through dehydration. Thus, it is significant to modify the rheological behavior of the solvent precursor for a successful sol-gel printing process. Li et al. proposed a simple heating method to evaporate water, achieving viscosity modulation of poly(3,4-ethylenedioxythiophene) polystyrene sulfonate (PEDOT:PSS) and PVA composite hydrogel.[67]

By controlling the solid content of the suspension (from 1% to 3%), the viscosity of the PEDOT:PSS aqueous solution increased from 25 mPa s−1 to 174 mPa s^{-1}, indicating the feasibility of injectable printing for biosensors. Besides, in a fixed system, the viscosity can be modulated by reconstructing the molecular structure of crosslinking agents, resulting in variations in sol-gel temperatures. Polyphenol-assisted gelation combines hydroxyl-rich biocompatible polymers with polyphenol compounds through dynamic physical bonding and can obtain different sol-gel transition temperatures with various topologies.[55,68] Luque et al. proposed that using plant-derived pyrogallol can achieve a modulable reconstruction temperature by changing the quantities of phenolic hydroxyl groups.[55] As a result, thstrong PVA-gallic TCN is equipped with near-covalent elastic moduli and a suitable sol-gel transition temperature for injection printing.

2.1.2. Freeze-Thaw Cycling

Freeze-thaw assisted hydrogen reassembly, untangling the initial crosslinked network by thawing and boosting regulated molecular arrangement by freezing, is a strategy to increase crosslinking points, enhancing resilience and anti-swelling/dehydration of ion gels by repeated solid-gel transitions (Figure 2c).[72–76] As the number of freeze-thaw repetitions increases, the crosslink density within the hydrogel increases, sacrificing the flexibility of the gel for improved elasticity. Borates and phosphates are the conventional utilized micromolecular crosslinkers, benefiting from their stable molecular structures with polyhydroxy units. Nevertheless, owing to the strong hydrogen interaction,

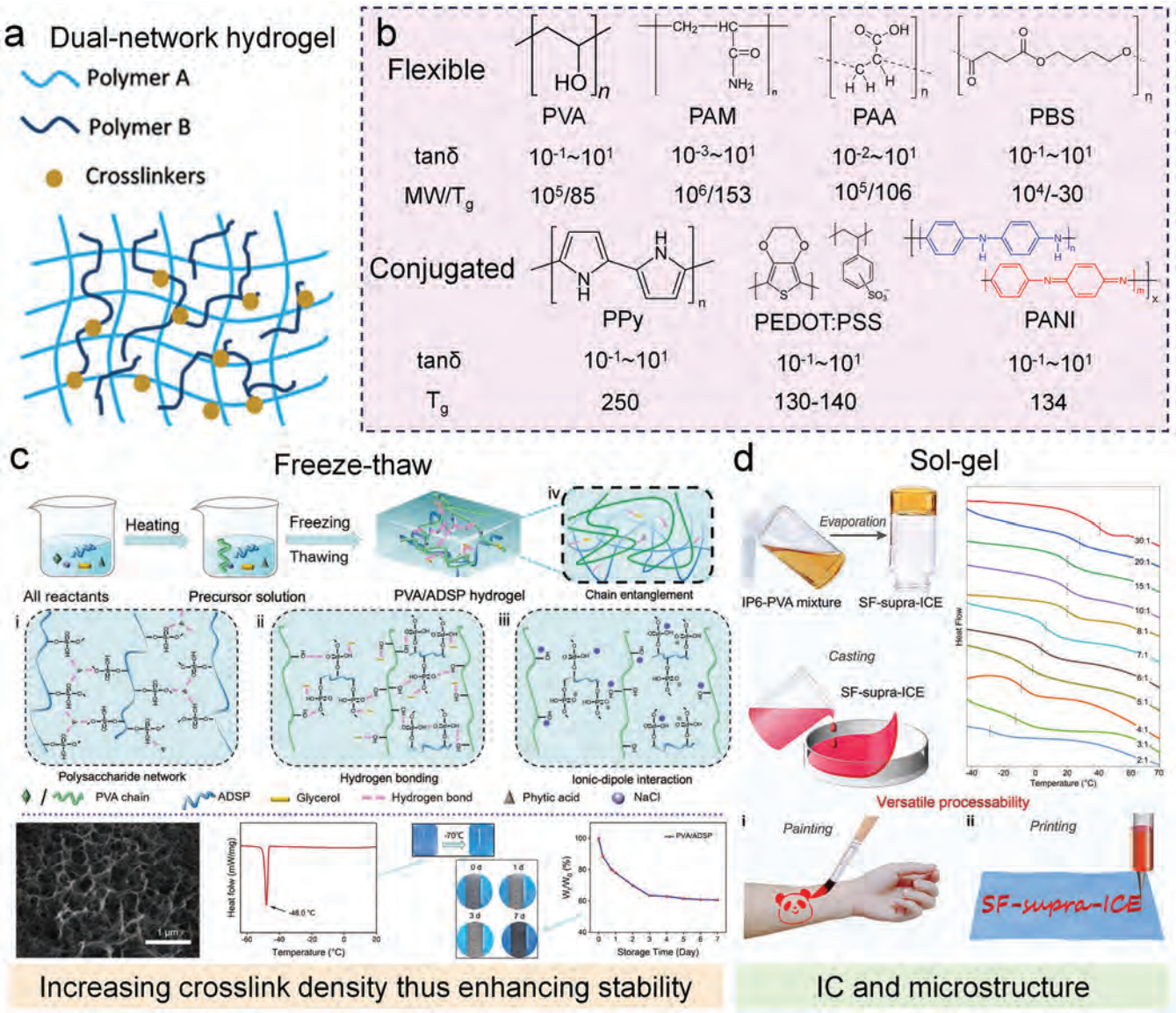

Figure 2. a) Illustration of dual-network hydrogel.[69] Reproduced with permission. Copyright 2024, Wiley-VCH GmbH; **b**) Common polymers utilized in hydrogel systems with their molecular information.[52,55,57,60,65,70,71]; c) Freeze-thaw cycling method, with the morphology of porous structure and stability of the ion gels.[72] Reproduced with permission. Copyright 2024, Elsevier; d) Sol-gel transition method, with DSC curves of the ion gels under different water content.[56] Reproduced with permission. Copyright 2023, Wiley-VCH GmbH.

the poor flexibility of the fabricated ion gels impedes further bioelectronic applications such as body movement sensing or tactile perception.[77] Zhu et al. combined the salt-immersion process with a freeze-thaw method to simultaneously endow the hydrogel with superior elasticity (elongation at break: 8.18 times), environmental stability, and ionic conductivity (3.59 S m^{-1}), displaying great responsibility (128 ms), sensitivity (Gauge Factor (GF) = 1.82 at 350%–500% strain) and durability while acting as a strain sensor.[72] Notably, this physical crosslinking method can avoid toxic reagents and provide a facile strategy to construct a crosslinked network with microstructures. As reported by Pan et al., by conducting several freeze-thaw cycles, the fabricated PVA hydrogel microneedles possessed excellent elasticity and mechanical properties, which are conducive to stable drug release.[73] In addition, multifunctional ion gels with dual-network or even triple-network can be facilely constructed by repeated freeze-thaw cycles, such as PVA with Gellan gum (GG), polyetherimide (PEI), sodium glycinate (SG), and starch.[64,74,75,78]

2.1.3. Performance Comparison

Sol-gel transition and freeze-thaw cycling can reassemble hydrogen bonding by modulating the viscoelasticity of ion gels, solving the engineering challenges for IC/microstructure printability (Figure 2d) and environmental stability (Figure 2c), respectively. Hydrogels assembled by freeze-thaw cycling possess

Table 1. Mechanical and electrical properties of dual-network hydrogel.

Method/Interaction	Material	R_m [MPa]	δ [%]	σ [S m^{-1}]	Ref
Sol-gel (H-bond)	PVA/IP6	12.5	573	0.045	[56]
	PVA/PPy	9.4	36	8000	[57]
	PVA/PBS/LiCl	5.52	653.6	8.3	[65]
	PVA/kC	0.054	117.81	50	[66]
	PVA/PEDOT:PSS	2.5	25	0.004	[67]
	PAM/Chitin-graft-PANI	0.84	1303	4.8	[59]
	PAM/Chitin	0.214	1586	0.62	[80]
	PAM/CD	0.109	5443	0.29	[70]
Freeze-thaw (H-bond)	PVA/CD	0.5	314	2.48	[58]
	PVA/PANI	0.05	170	40.8	[60]
	PVA/SPI	1.4	772	1.46	[63]
	PVA/Starch/Gly	0.53	793	1.00	[64]
	PVA/Gly/ADSP	2.26	818.6	3.59	[72]
	PVA/TA/GG	1.2	891	3.27	[74]
	PVA/PEI/Gly-Na	2.2	386	5.54	[75]
	PVA/Gly-acid	0.55	510	5.11	[76]
	PVA/Starch/[Emin]Ac	0.53	580	2.75	[78]
	PVA/PU	6	680	1	[81]

Abbreviations: ADSP: acetylated distarch phosphate; CD: cyclodextrin; Gly: glycerin; kC: k-carrageenan; PBS: polybutylene succinate; SPI: soy protein isolate; [Emin]Ac: 1-ethyl-3-methyl imidazolium acetate; Rm: tensile strength; δ: elongation; σ: conductivity.

environmentally friendliness compared with chemically crosslinked hydrogels, which are suitable for application scenarios requiring hydrogel exposure to air, such as humidity/temperature sensors for tactile perception. Compared with the freeze-thaw method, the advantages of sol-gel transition are fast molding and shape-mouldability. At the same time, mechanical matching (tanδ) and magnificent differences of T_g between the two molecules are essential to avoid phase separations in processing and provide wider temperature windows for mechanical/electrical properties modulation. For instance, tanδ of PVA, and PPy share the same magnitude (10^{-1}~10^{1}) and different T_g (85°C and 250°C), indicating good mechanical matching and superior performance of PVA/PPy hydrogel system (Figure 2b and **Table 1**).

Typically, hydrogels composed of two linear polymers with flexible and conjugated segments (PVA/PPy, PVA/PANI, and PVA/PEDOT:PSS), respectively, possess superior mechanical strength and conductivity compared with flexible-polymer/ion-liquid material systems (Table 1). Besides, compared with linear-linear combination, linear-cyclic dual-network hydrogel (PAM/CD) possesses higher stretchability (5443%) but lower tensile strength at breaking (0.109 MPa), due to the relatively free motion of cyclic molecules. Additionally, the coexistence of covalent and hydrogen-bond crosslinking points of dual-network hydrogel allowed it to exhibit more comprehensive performance than static crosslinked networks, showing high toughness and network stability (**Figure 3a**). Apart from the favorable processability, stability, and conductivity, dual-network hydrogel typically possesses spectra-transparency, broadening the applications in see-through electronics, invisible soft robotics, and other optical fields such as contact and liquid lenses, in vivo optical sensors and body-contact optical fibers, as well as smart windows for temperature, electrical and humidity control (Figure 3b).[70,80–82]

2.2. Nanocluster-Strengthened Crosslinked Structure

Topological nanoclusters (i.e., branched supramolecular nanoparticles) are generally utilized to enhance the mechanical properties and electrical conductivity of the ion gels by assembling star, branched, and dendritic monomers with crosslinkable terminal groups.[15,83–85] Compared with linear polymer skeleton, ion gels with branched crosslinked structures possess higher crosslinking density through multi-connection between molecular arms, thus enabling unique rheological properties of the fabricated bioelectronics.[24,86] However, the hydrogen-bonding interaction between the macromolecular chains is relatively weak, which requires external cross-linking stimuli, such as photoinitiation or polymerization by acclimatization rather than simple mechanical triggering.[54,87,88] Owing to plentiful sacrificial bonding inside the nanoparticles, ion gels possess superior tensile strength and stretchability. According to the different molecular interactions, the assembly strategy of topological clusters can be categorized as host-guest interaction and metal-ligand coordination, and the illustration of the TCN is shown in **Figure 4a**. To optimize the reactant ratios, the molecular information of staple organic ligands and host/guest molecules needs to be clarified (Figure 4b).

2.2.1. Metal-Ligand Coordination

Metal-ligand coordination, typically utilizing transition metal atoms as the allotropic center and organics containing lone-pair electron functional groups as the ligands, is a facile synthesis method to construct branched supramolecular nanoparticles.[54,89,90] Polyphenol-like biological extracts and their monomeric derivates, classified as tannic acid (TA), caffeic acid (CA), gallic acid (GA), ellagic acid (EA), catechol, and lignin, are the conventional coordinated ligands, owing to their hydroxyl-rich characterization, resource extensivity, high biocompatibility, ease of modification and degradation.[84,85,91] For instance, Fe^{3+} and catechol could be mixed to construct the crosslinked network, forming magneto nanoparticles (Fe_3O_4) (≈50 nm) by in situ mineralization, resulting in mechanical reinforcement and defects minimization of ion gels with a small number of minerals.[85] Besides, monophenols can be coordinated with metal ions and crosslinked with long-chain macromolecules to form high-strength ion gels, owing to the higher specific surface hydroxyl functionality and rigid bi-lactone structure. TA undergoes molecular reorganization in synthesizing monophenols by hydrolyzing them into GA first and then forming sheet-like EA structures under ultrasonication. Additionally, through Fe^{3+} ions mediated assembly, the phenolic ligands are constrained by the coordination of Fe^{3+} to establish a homogenous nanostructure.[54] Benefiting from the regular morphology of nano-assemblies (≈35 nm), the photocured ion gel possessed ultra-robust mechanical properties and molecular flexibility, capable of body motion sensing and health monitoring under severe environmental conditions (Figure 4c).

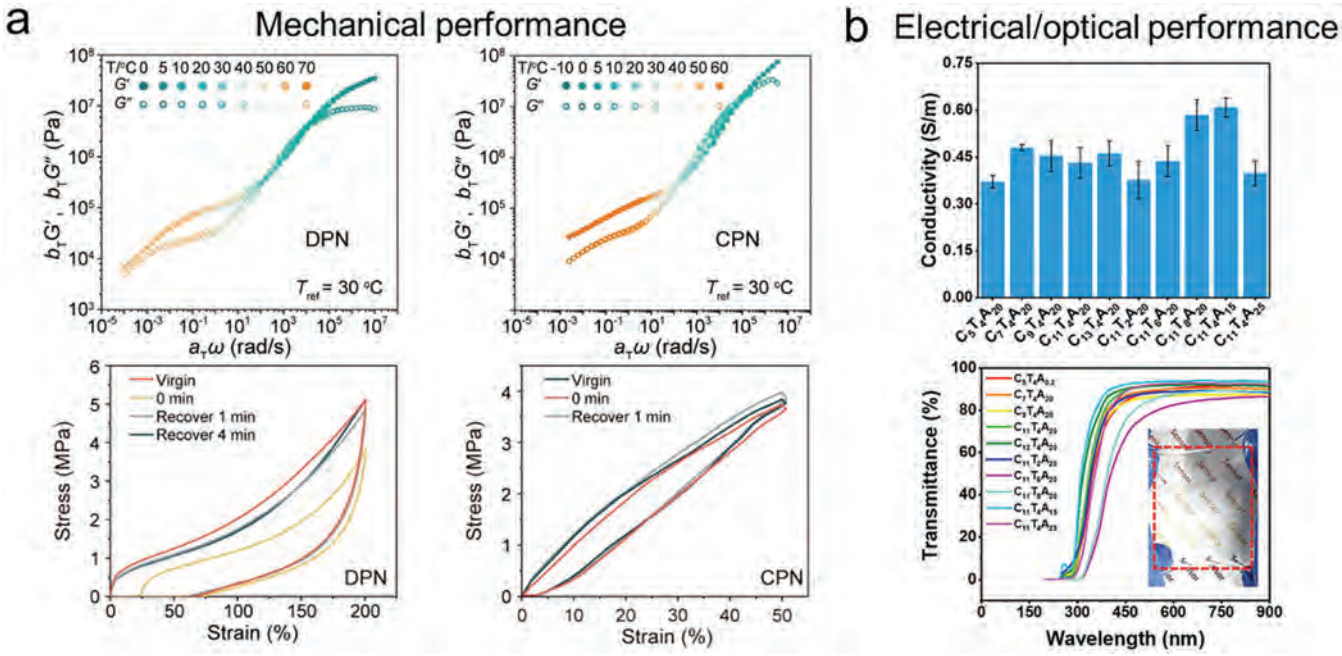

Figure 3. a) Mechanical performance comparison between the dual-polymer network (DPN) and covalent polymer network (CPN), indicating the enhanced toughness and more crosslinking points of the dual network hydrogel.[79] Reproduced with permission. Copyright 2023, Wiley-VCH GmbH; b) The electrical/optical performance of the dual-network hydrogel shows great stability and transparency while working as an electronic device.[80] Reproduced with permission. Copyright 2022, Springer Nature.

2.2.2. Host-Guest Interaction

Host-guest interaction is a method of assembling different functional molecules or polymers onto the surface of nanoparticles through noncovalent interactions between molecules (e.g., hydrogen bonding, π-π interactions, electrostatic interactions).[23,88,93] Cyclodextrins (CDs), a class of cyclic oligosaccharides composed of glucose units possessing superior molecular recognition ability (since hydrophilic and hydrophobic groups of CDs are capable of recognizing the corresponding groups with similar affinity, respectively), are commonly used host molecules for responsive nanocluster assembly.[94,95] Through noncovalent interactions, the CD can be crosslinked with hydrophilic molecules like polyethylene glycols (PEG), PAM, and gelatin or acrylic-esters such as glycidyl methacrylate-1-adamantanamine (GMA-Ad).[22,88] Additionally, combined with the electrical conductivity and flexible topological network of the ion gels, the sensors are equipped with extremely high sensitivity as biosensors or strain sensors. For instance, Chen et al. synthesized PEG/β-CD topological nanoparticles by isocyanate chemistry and dialysis (≈530 nm), which afterward hydrogen bond-crosslinked with GMA-Ad skeleton, the PEG/β-CD nanocluster-strengthened strain sensor displayed a wide sensing range of 0%–1800%, enabling comprehensively monitoring of human activities (Figure 4d).[88] Notably, the modulation between stiffness and elasticity of ion gels depends on nanoparticle crosslinkers' size. Wang et al. proposed a three-component supramolecular approach to control nanoparticle size, including Ad-grafted polyamidoamine as dendrimer center/core, β-CD-grafted branched PEI as propagation groups, and Ad-functionalized PEG as solvation groups.[93] The size of supramolecular nanoparticles can be altered by tunning the mixing ratio of propagation/solvation groups (≈30–450 nm).

2.2.3. Performance Comparison

As for the assembly of nanoclusters, the advantages of the metal-ligand method are gentle reaction conditions and green and facile fabrication, while the removal of spare ligands and purification of nanoclusters are problematic. On the other hand, although host-guest chemistry has a high molecular recognition capability and can precisely regulate the reaction process through specific host-guest interactions, resulting in nanoparticles with controllable size and morphology, there are still technical issues such as the limited choices of host molecules, precise structural modulation during chemical synthesis, high costs of partial chemicals (CDs) and difficulties in scale-up fabrication. The introduction of nanoclusters decouples the competing effects between tensile strength (30.9 MPa) and conductivity (0.01 S m^{-1}) through relatively robust metal-ligand interaction, while the host-guest nanoassemblies made by CD enhance the stretchability (1860%) of the ion gels (**Table 2**). Compared with branched topological nanoclusters (metal-polyphenol), cyclic molecules possess a more free volume of segments, thus suitable for wearable/flexible bioelectronics. The robust ion gels fabricated by metal ligands are proficient in organization engineering for neuronal regeneration and impact-resistant protective materials. Except for mechanical sensing, the photoluminescence of ion gels is a critical index owing to the fastest response time of photons, which can provide an optical detecting mode for strain sensing and biosensing. For instance, Song et al. modulated the band structures

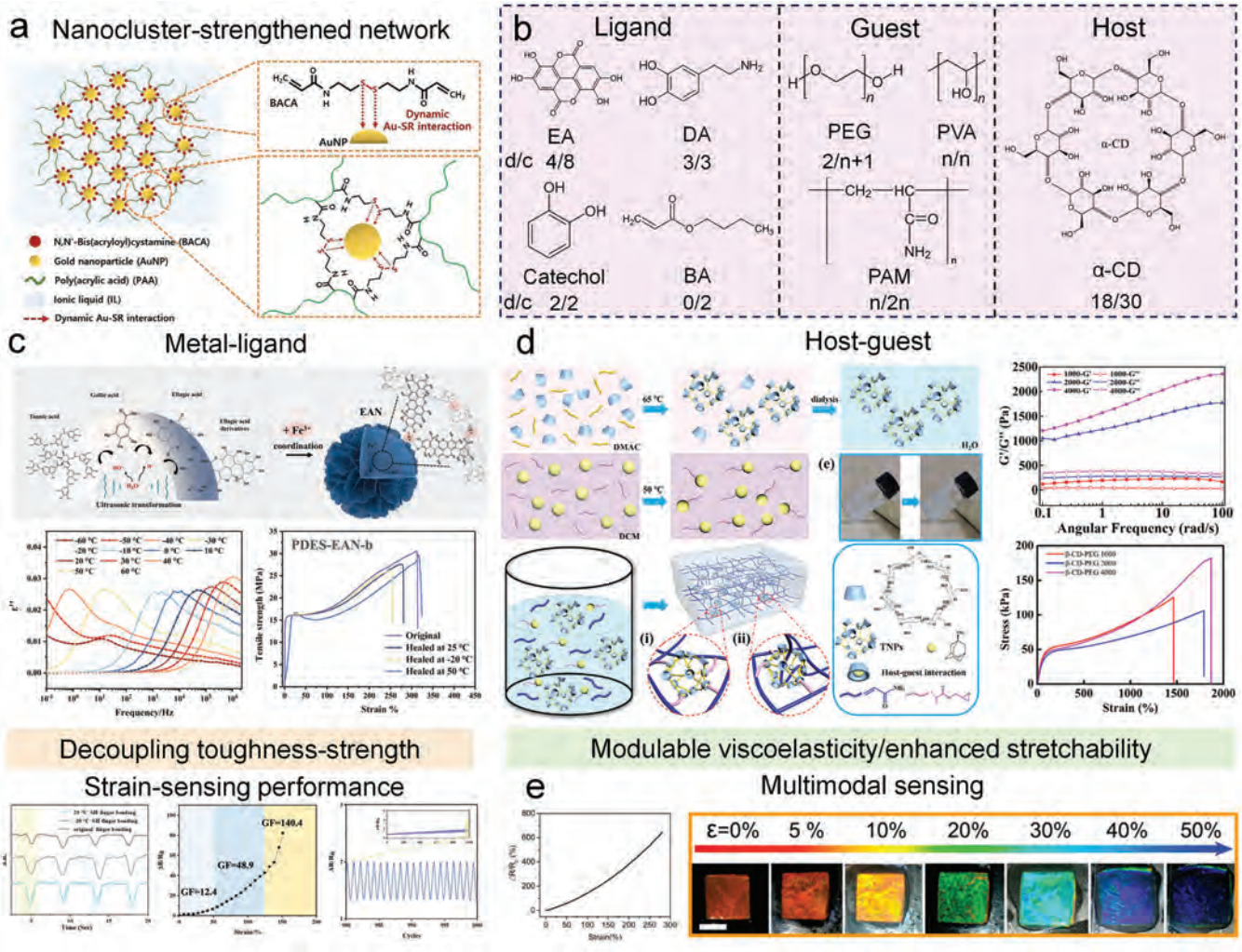

Figure 4. a) Illustration of nanocluster-strengthened network.[90] Reproduced with permission. Copyright 2023, Elsevier; b) Crosslinking donors and coordination sites of the commonly used components; c) Metal-ligand method. The dielectric/tensile test and sensing performance of the ion gels demonstrated great molecular flexibility and mechanical enhancement.[54] Reproduced with permission. Copyright 2023, Springer Nature; d) Host-guest reaction. The rheological behavior and tensile test reflected the modulable viscoelasticity and enhanced stretchability of the crosslinked network.[88] Reproduced with permission. Copyright 2021, Elsevier; e) Multimodal (strain-photoluminescent) sensing.[92] Reproduced with permission. Copyright 2021, American Chemistry Society.

and optical properties of quantum dots by controlling the size, and realizing the concentration monitoring of hydrazine as a result.[96] In addition, the intensity and wavelength of photoluminescence can be modulated through ligands and metal transformation, respectively.[97] With the abovementioned strategies, bioelectronics with superior sensing performance and reconfigurable physical properties can be fabricated, indicating the multimodal sensing capability and application of fluorescence diagnostics (Figure 4e).

2.3. Slide-Ring Crosslinked Structure

Mechanically interlocked polymers (MIPs), utilizing dynamic physical bonds to modulate the degrees of freedom in polymer architectures, have opened new avenues for developing reconfigurable polymers, particularly in molecular machines like switches and sensors.[103] Depending on the placement of the components (within leading chains, side chains, or crosslinkers), rotaxane units profoundly affect material properties.[103] Among these, slide-ring crosslinked networks (SRGs), a critical MIPs category where rings can freely move along the axle, form figure of '8' crosslinking structures that slide along polymer chains, redistributing tension and enhancing properties like stretchability, adhesion, and swelling (**Figure 5**a). For example, a type of polyrotaxanes (PR) proposed by Jiang et al., where multiple cyclic β-CDs are threaded onto PEG and prevented from detaching by bulky end stoppers, is the typical slide-ring supramolecular network that simultaneously enhances stretchability, interfacial compatibility and ductility of biosensors.[32] The assembly mechanisms (i.e., ring-chain interactions), commonly classified as metal-ligand coordination, hydrogen bonding, and π-π stacking, significantly influence the viscoelasticity of ion gels.

Table 2. Mechanical and electrical properties of nanocluster-strengthened crosslinked network.

Method/Interaction	Material	R_m [MPa]	δ [%]	σ [S m^{-1}]	D [nm]	Ref
Metal-ligand	PAM/BA@Fe^{3+}	3	600	0.059	NA	[98]
	ENR/PDA@Fe^{3+}	1.9	108.7	0.03	NA	[99]
	PDES/EA@Fe^{3+}	30.9	275	0.01	≈35	[54]
	PEG/Catechol@Fe_3O_4	0.03	120	NA	≈50	[85]
	PHEMA/Lignin@Fe^{3+}	0.184	1976	1.99	≈128	[91]
	HA/IM@Ni^{2+}	5.68	600	6.863×10^{-2}	≈1	[100]
	PAA/BACA@Au	0.015	800	0.2	≈10	[90]
	PEO/PS@Li^+	1.4	NA	9.5×10^{-3}	≈1.91	[101]
Host-guest	PAM/PEG/γ-CD	1.05	1000	NA	≈5	[22]
	PVA-Ad/CD/EGaIn	NA	800	1.58×10^4	≈500	[23]
	PVA/Gelatin/P(β-CD)	0.054	778	1.67	NA	[30]
	PVA/Gelatin/β-CD	0.025	1200	6.4	NA	[31]
	PEG/GMA-Ad/β-CD	0.18	1860	0.24	≈530	[88]
	Polyurea/HCA	3.5	495	1.85×10^{-2}	≈30	[15]
	CNF/CNC/PIL	6.2	260	0.62	≈50	[102]
	PDAAM/HP-A	0.365	1170	0.16	NA	[86]

Abbreviations: PEO/PS: polyethylene oxide/polystyrene; BA: butyl acrylate; ENR: epoxidized natural rubber; PDA: polydopamine; PDES: polymerizable deep eutectic solvent; HA: 2-hydroxyethyl acrylate; IM: 1-vinylimidazole; PAA: poly(acrylic acid); BACA: N, N'-bis(acryloyl)cystamine; CNF/CNC: cellulose nanofiber/nanocrystal; PDAAM/HP-A: poly(diacetone acrylamide)/acrylate-terminated hyperbranched polymer; PHEMA: poly(2-hydroxyethyl methacrylate); EGaIn: indium gallium eutectic; HCA: hyperbranched cluster aggregates; Rm: tensile strength; δ: elongation; σ: conductivity; D: size of nanocluster.

2.3.1. Metal Template Technology

Template strategy is currently the primary method for synthesizing SRGs, assembling components through supramolecular interactions, followed by a capture reaction (e.g., ring closure or the introduction of terminations) to form dynamic crosslinking bonds.[104] Metal-ligand coordination, which can endow ultra-robust mechanical properties, dynamic tunability, and temperature/chemical responsiveness to ion gels, is the most frequently utilized template for SRG synthesis.[105] Additionally, the coordination technologies are used in passive and active metal template methods, which aim to assemble components for orientation and provide control over the dynamic bond conformation, respectively. For instance, Stoddart and his co-workers first raised the concept of mechanically interlocked molecules by utilizing passive metal templates; besides, proposed by Bai et al., a dynamic oligo[2]rotaxane network was obtained from a [2]rotaxane molecule through copper (I)-catalyzed polymerization, which possessed superior toughness, stiffness, and flexibility, benefited from the active metal-ligand coordination.[105] Subsequently, Ghiassinejad et al. systematically analyzed the locking effect of the rings by palladium ions by modulating the ion concentration and controlling ring mobility to affect the storage and loss moduli of the ion gels (Figure 5b).[106] Accordingly, the metal-ligand interlocking is a facile strategy to construct SRGs with stimuli-reconfigurability, promising future application in biosensing.

2.3.2. Hydrogen Bonding

Hydrogen bonding is similarly employed not only for threading of polymer chains through cyclic molecules but also for wrapping a circle to an axle, and the commonly used molecules are illustrated in Figure 5c (the information of PEG, PAM, and CD ring can be viewed in Figure 4). For example, crown ethers are used to thread linear molecules through macrocycles, depending on the weak complexation of hydrogen bonding between the rings and axle. Gibson et al. reported a novel PR synthesized by condensation of di-acyl chloride with 1,10-decanol in the presence of 30-crown-10 and, afterward, double-termination of triphenylpropionyl chloride-hydrolysis reaction capping.[107] Additionally, ring mobility can be controlled by chemical (cation templates) or physical stimuli (light or electrochemical inputs).[108] For instance, Takata et al. linked crown ether rings to polymer chains via click chemistry (ammonium group-crown ether pairs) to form stable PR, regulating ring mobility through interactions between the axle and the ring.[109] Besides, the treading of axle and CD inclusion complexes can be effectively processed by combining the hydrophobic effects between the linear polymer and CD circles and the hydrogen bonding between adjacent CD rings. Consequently, except for PEG, CD-based PR with various polymers have been reported, e.g., poly(propyleneglycol) (PPG), poly(ethylene oxide) (PEO, high molecular weight PEG), and poly(isobutylene) (PIB).[32,34,110–113] However, the free motion of the ring may lead to phase separation; in addition, the strength of hydrogen bonds is sensitive to humidity and solvent polarity. Thus, encapsulation and segregation will be required for the practical application of bioelectronics.

2.3.3. π-π Stacking

π-π stacking and charge transfer interactions have also been adopted to construct PR, particularly involving cyclobis(paraquat-p-phenylene) ($CBPQT^{4+}$) as a cyclic component.[114] Stoddart and colleagues synthesized PR containing 1,5-dioxynaphthalene

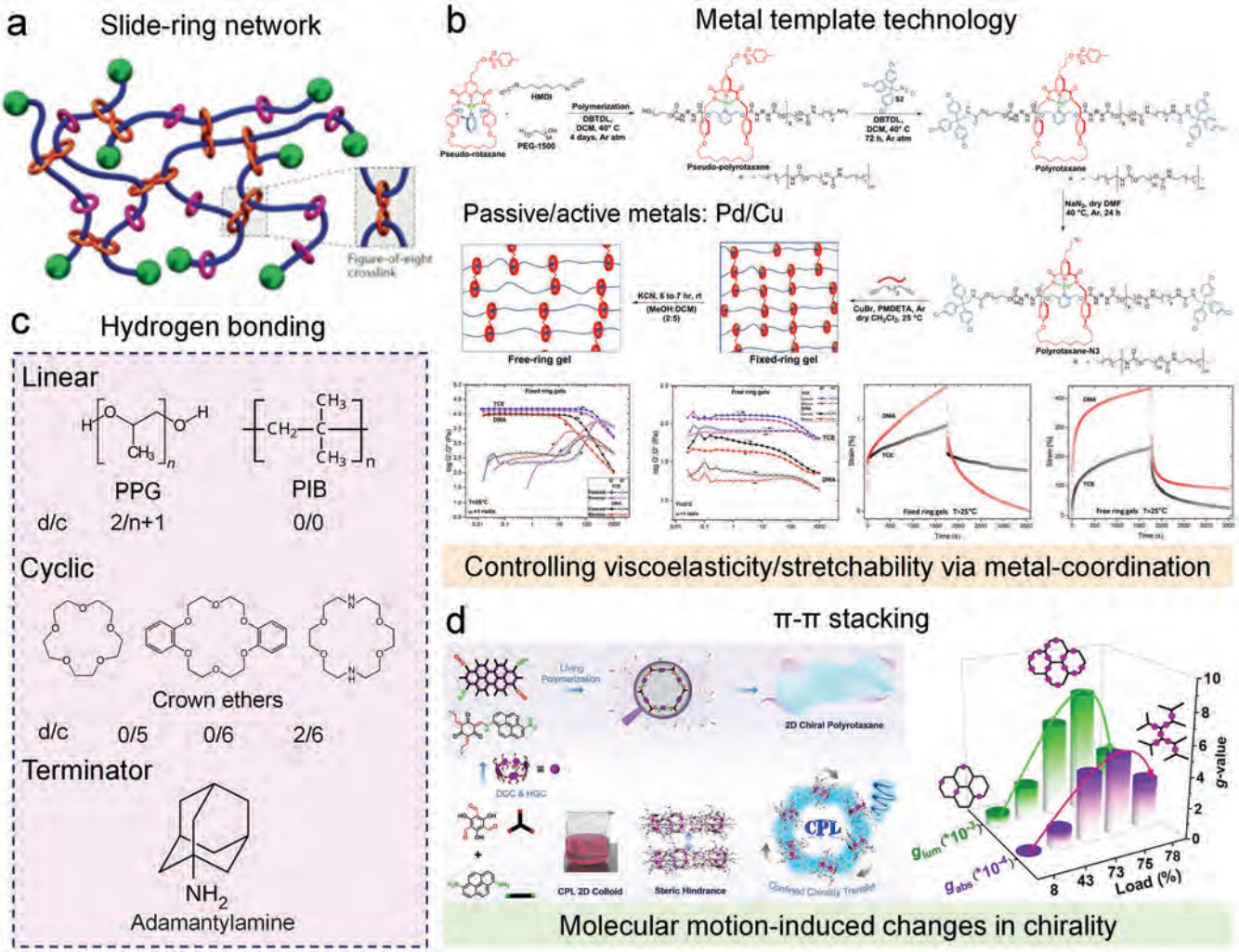

Figure 5. a) Illustration of the slide-ring network.[103] Reproduced with permission. Copyright 2024, Elsevier; b) Metal template technology. The rheological behavior/viscoelasticity comparison between fixed-ring gels and free-ring gels.[106] Reproduced with permission. Copyright 2024, American Chemical Society; c) Crosslinking donors/coordination sites of commonly used molecules for hydrogen bonding method; d) π-π stacking method.[25] Reproduced with permission. Copyright 2021, Wiley-VCH GmbH.

(DNP) units as π-electron donors and $CBPQT^{4+}$ as acceptors, resulting in robust, dynamic folding of the ion gels.[115] Besides, 2D conjugated molecules are interlocked by rings through π-π stacking, preventing self-aggregation of 2D molecules and providing structural modularity by controlling the feeding amount of ring, thus endowing unique optical properties of the gels (Figure 5d). Hu et al. proposed a novel π-π stacking strategy for fabricating single-layered 2D polymeric materials with chirality photoluminescent activity.[25] This device was prepared using β-CD as a chiral macrocyclic wheel and a dynamic framework 1,6-diaminopyrene as the luminescent axle. The effect of β-CD prevents the π-π stacking between the adjacent 2D conjugated molecules, avoids the aggregation-caused quenching, and incorporates supramolecular chirality into the polymeric network. Accordingly, the motion of β-CD enables chirality modulation.

The properties of SRGs are closely related to the mobility of their crosslinking points, where the free movement of the rings provides enhanced stretchability (**Table 3**), resilience, and other reconfiguration-induced unique properties. The relationship between ring mobility and ring-chain interaction in these systems is crucial for developing materials with novel functionalities, broadening the application field of bioelectronics, such as drug delivery and mechano-luminescence. However, bioelectronics based on

Table 3. Mechanical properties of slide-ring crosslinked network.

Method/Interaction	Material	R_m [MPa]	δ [%]	Ref
Metal-ligand	Oligo[2]rotaxane/Pd^{2+}	1.58	275	[105]
	PEG-1500/HMDI/Pd^{2+} (fixed)	0.1	167	[106]
	PEG-1500/HMDI/Pd^{2+} (free)	0.1	3200	[106]
H-bond	Ad-PEG-Ad/CD	50	150	[32]
	PAM/Ad-PEG-Ad/CD	0.156	740	[34]
	ACA-PEG-ACA/CD	3	2540	[113]

Abbreviations: ACA: acrylamide; HMDI: hexamethylene diisocyanate.

SRGs is beset by a synthetic problem (i.e., controlling ring numbers and precise structural modulation). Compared with hydrogen bonding and π-π stacking, the interaction strength of metal-ligand coordination is stronger. Yet, using heavy metal ions is not conducive to implantable bioelectronic application. Additionally, the higher mobility of rings may cause undesirable stability of carrier conduction in the aspect of biosensing.

3. Conductance Mechanism in TCNs

In addition to providing the feasibility of circuit printing and microstructure processing, decoupling competition between mechanical and electrical properties, and enhancing elasticity, TCNs can also achieve conductance modulation by molecular reconfiguration. While our understanding of the conduction mechanisms in TCNs is primarily ionic transport in polymer hydrogels or polyelectrolytes, we initially focused on elucidating the underlying physical processes in conventional organic conductors. Detailed descriptions of the conduction mechanism can be found in the scientific literature.[116] Furthermore, we elaborate on the ion-dominant transport mechanism in TCNs from the perspective of reconfigurable molecular interaction.

3.1. Electronic Transport

Electronic transport, occurring mainly in the conjugated systems, is intermediate between intramolecular band transport in the ordered conjugated phase and intermolecular hopping transport in the amorphous phase.[117] In organic conductors, intramolecular transport of electronic charges occurs alongside the π-π conjugated molecular chains through electron delocalization of p-orbitals. In contrast, intermolecular transport is governed by the overlap of p-orbitals between adjacent molecules[116,118] (**Figure 6a**). The discontinuous transport pathway of intermolecular transport leads to low electronic charge mobility and electrical conductivity compared with ordered band transport. For most conjugated polymers, owing to the weak intermolecular force resulting from a high degree of π-conjugation, static or dynamic molecular disorders generally happen, resulting in the dominance of thermally activated hopping and thus declining conductance in organic conductors[119] (Figure 6b).

Based on the types of leading carriers, organic semiconductors can be categorized into n-type and p-type, which are utilized as the channel layer for organic field effect transistors (OFETs) and organic electrochemical transistors (OECTs).[117] The devices with n-type semiconductors are fast-response with a high on-off ratio. At the same time, environmental stability is a critical issue due to the material defects and interactions between electrons and air molecules. On the other hand, p-type semiconductors are more stable for long-term use, while the sensing performance is worse than n-type.[119] The fabrication processes of organic semiconductors contain evaporation of small molecules in a vacuum, casting of polymer solutions, and stripping of feedstock single crystals to substrates.[119] After deposition of the channel layer on source-drain electrodes, ion gels with dynamic crosslinked networks are typically coated on the channel as a gate dielectric layer, forming an electronic double layer (EDL) to control the energy band structure and electronic transport of the channels (Figure 6b)[118]. Besides, electrochemical doping can influence the density of electronic carrier charges by the ionic-electronic coupling effect, hence realizing conductance modulation of the conjugated crosslinked network.[42,118]

3.2. Ionic Transport

Ionic transport is more complex than electronic transport, whose mechanisms are related to the molecular/ionic categories and solvent content/compositions and can be classified as ion hopping, solvent/vehicle mechanism, and Grotthuss mechanism.[120–123]

3.2.1. Ion Hopping

For organic conductors, the transport capability of the ion channel is one of the critical indexes to evaluate the sensing performance of bioelectronics. In the dry state (nonsolvent), ion hopping is the dominant mechanism of ionic migration, dependent on the mobility of backbone segments and side-chain groups in the crosslinked network (Figure 6c). Molecular flexibility is related to the intrinsic chemical structures (C-C double bond is more rigid than C-C single bond) and molecular free volume (intermolecular force) of the crosslinked skeletons, which can be modulated by the soft/rigid segmental ratio and temperature, respectively.[124] For instance, heterogenous blends or copolymers (microphase segregation) and homogenous conjugated polyelectrolytes (without segregation) were synthesized to control the soft/rigid ratio, thus enhancing ionic-electronic coupling and capability of conductance modulation.[60] Additionally, molecular segments are frozen below Tg, resulting in low hopping efficiency, while high ionic mobility occurs when the temperature is above T_g.[78] Accordingly, the ionic conductivity (σ) can be expressed regarding temperature-dependent functions in organic conductors with fixed chemical structures. Depending on the relationship between environmental temperature and T_g, ionic conduction can be defined as molecular viscosity-guided hopping (Arrhenius equation,[125] 1) and thermally activated hopping behaviors (Vogel-Tammann-Fulcher equation,[126,127] 2):

$$\sigma = \sigma_0 \, e^{\frac{-E_a}{k_B T}} \quad \left(T \le T_g\right) \tag{1}$$

$$\sigma = \sigma_0 \, T^{-\frac{1}{2}} e^{\frac{-E_a}{k_B (T - T_0)}} \quad \left(T > T_g\right) \tag{2}$$

where σ_0 denotes a preexponential factor. E_a and k_B represent the activation energy and Boltzmann constant, respectively. T and T_0 are the given temperature and a reference Vogel temperature (equal to T_g in ideal conditions), respectively. As demonstrated in Equations (1) and (2), ionic conductivity and temperature are positively correlated within a certain range, indicating the significance of modulation in T_g (molecular flexibility) for high ionic conduction performance.

3.2.2. Solvated Mechanism

Solvent plasticization, weakening intermolecular interactions to reduce viscosity (e.g., plasticization of PVA by water or glycerin),

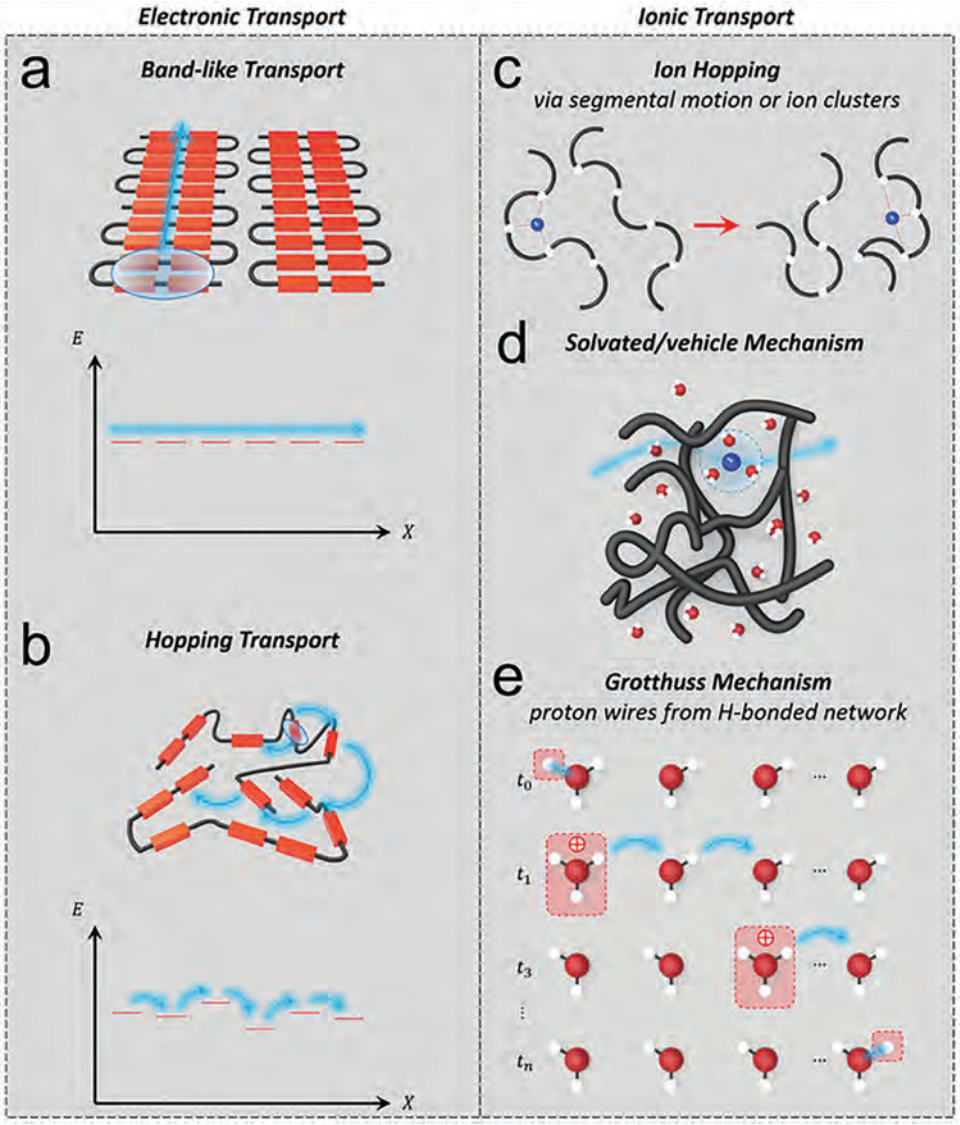

Figure 6. a) Band-like transport in conjugated systems; b) Thermally activated electron-hoping occurred in amorphous regions; c) Ion-hoping in a dry state; d) Solvated/vehicle mechanism in the gel state; e) Grotthuss mechanism for proton transport. Reproduced with permission. Copyright 2023, Wiley-VCH GmbH.

is another mechanism to enhance the ionic conductance of organic ionic conductors (Figure 6d).[127] Except for viscosity reduction-induced promotion of ion hopping, in the swollen and gel states of organic conductors, solvents can be the channels carrying organic/metal ions through coordination interaction.[128] Polar solvents, with higher solvation capacity, promote the separation of anions and cations of ionic liquids and polyelectrolytes, thus facilitating ion transport, especially of protons (some polar solvents are also intensely nucleophilic, which prevent proton bursting by polymer backbone groups[129]).

3.2.3. Grotthuss Mechanism

For instance, in the case of the proton as the charge transport carrier and water as the solvent, the proton will fast diffuse and transport through the Grotthuss mechanism (coordination bond exchange) between water molecules or polymer-water hydrogen bonding networks[130] (Figure 6e). To assess the ion transport efficiency in organic conductors containing solvents, the ionic concentration, ionic valence, ionic mobility, and ionic diffusion coefficient must be considered. Similar to electronic transport, ion transport can be classified as the cation (hole) and anion (electron) tunneling and quantified by the parameter of σ, which is the sum of ionic conductivity provided by each ionic variety (i)[131]:

$$\sigma = \sum_i n_i \left| z_i \right| \; e\mu_i \tag{3}$$

where n_i, z_i, and e represent the ion concentration, ion charge, and elementary charge, respectively. Additionally, μ_i is ion

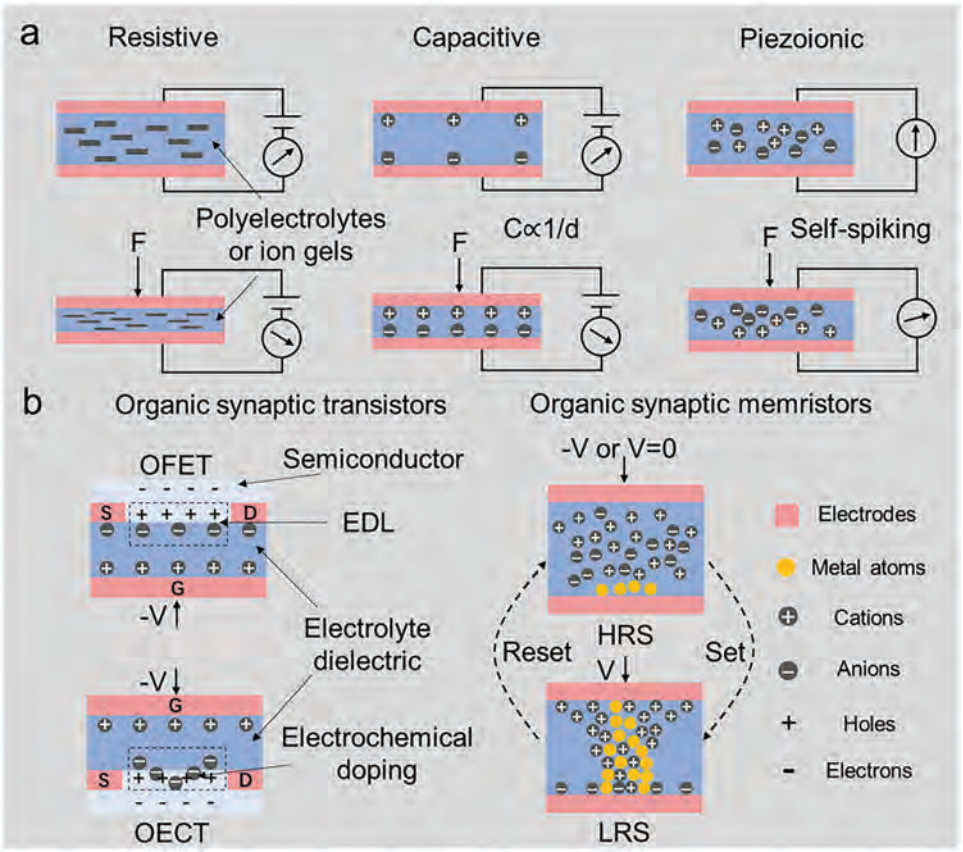

Figure 7. a) The main sensing mechanisms (modes) of strain sensing devices based on ion-dominant transport; b) Synaptic devices can be divided into organic field effect transistors (OFETs), organic electrochemical transistors (OECTs), and organic synaptic memristors. HRS: high resistance state; LRS: low resistance state.

mobility, which is convertible to diffusion coefficient (D_i) via the Nernst-Einstein relation[131–133]:

$$D_i = RT\mu_i \tag{4}$$

where R is the gas constant, the above ion transport equations in solvent-borne organic conductor systems hold under the assumption of infinite molecular dilution. Yet, the ideal condition is not present in swollen or hydrogel states. Considering ion neutralization and aggregation, calculating σ is a nonlinear superposition; hence, the raw ion concentration in organic conductors is not informative. Instead, ions and molecules' thermodynamic activities are prioritized in determining ion transport efficiency. Distinct from conventional conjugated systems, TCNs possess more reconfigurable interactions such as hydrogen bonding, host-guest interaction, and metal-ligand coordination rather than only π-π stacking and van der Waals interaction, leading to topology-related transport mechanisms and new concepts for conduction modulation.[10,11,50,134]

3.3. Ion-Dominant Transport in TCNs

Dynamic response in TCNs is the reconfigurable behavior of conductivity changing in response to external stimuli (stress/electrical/optical pulses), whose mechanism can be divided into electronic-dominant and ion-dominant responses. Among these, sensors possessing ion transport channels similar to those of synaptic neurons are extensively applied in e-skin and wearable tactile perception systems. Based on sensing mechanisms, they can be categorized as resistive, capacitive, self-spiking sensors, and electrochemical synapse/neuron devices (**Figure 7**).[67,69,135,136] Equivalent electrical components and connections to ionic sensors can be obtained by electrochemical impedance spectroscopy (EIS) testing, and detailed mechanical analyses can be found in the scientific literature.[120] For resistive sensors, the mechano-responsivity (i.e., Gauge factor (GF): the ratio of relative change in electrical resistance R, to the mechanical strain ϵ) is one of the critical indexes to evaluate the device performance, while variation in capacitance by generating EDL is the significant factor assessing the performance of capacitive and self-spiking sensors.[137,138] Except for the stretchability of ion gels, ion conductivity is an indispensable property for high GF value and the rapid establishment of EDL. As mentioned in the last section, ion transport efficiency mainly depends on the molecular flexibility of the crosslinked network. In contrast, conventional bioelectronics is generally constructed by rigid conjugated polymers, enabling electronic transport through weakening ion transport.[139] Besides, the stability of the existing crosslinked network is environmental-dependent owing to

the swelling and dehydration, and the internal solvent of the crosslinked network is typically conducive to ion transport, leading to the competing effect between stable sensing performance and high sensitivity.

In order to combat the handicaps in flexible bioelectronics, it is vital to expound the relationship between ion transport and molecular reconfiguration/interaction. Here, we elaborate on the ion-dominant conductance modulation mechanisms from the perspectives of thermodynamic activity (intermolecular force: coordination interaction and hydrogen bonding) and incorporate recent advances in enhancing sensing performance in bioelectronics through topological supramolecular design.

3.3.1. Single-Ion Transport in the Slide-Ring Structure

Since the Nobel Prize for supramolecular chemistry and the invention of molecular machines, topological molecular and supramolecular electronics have garnered tremendous attention, especially for studying molecular thermodynamics and mechanisms of ionic/electronic transport.[140] The molecular host/guest can act respectively as ion/electron conducting bridges, or vice versa, and the conductance modulation is achieved by the host/guest mutual motion and molecular interaction, whose scenarios are quantum interference, gating effect, and the coupling of the formers.[119,141,142] Inspired by molecular machines, a crosslinked network with a slide-ring structure can control the ion migration through the sliding movement of rings, owing to the attendance of ions on molecules by coordination interaction (**Figure 8a**). For instance, Bao's group proposed a conductance enhancement strategy by separating PEDOT molecules and PSS ions utilizing the sliding movement of CDs, and the ionic skin possesses superior conductivity ($\approx 10^5$ S m^{-1}) and linear conductivity variation under 0%–100% strain as a result.[32] Additionally, as reported by Shen et al., the ordered arrangement of CD rings can also prevent the aggregation of PEDOT/PSS through coordination interaction between cations and CD molecules, which can be confirmed by the rheology behavior and transparency of the ionic hydrogels.[134] In contrast, anions are hardly transported alongside the slide-ring backbones but instead caged by the rings due to the steric effect. By utilizing molecular dynamic (MD) simulation, the radius distribution function (RDF) and coordination number between Zn^{2+} and oxygen atoms can be calculated, confirming the single-ion conduction through coordination effect instead of thermally activated ion hopping (Figure 8b).[143] The effect of coordination interaction on viscoelasticity and ionic mobility can be analyzed by variable temperature conductivity tests regulating the ratio of metal and oxygen elements (i.e., the ratio of paired electrons and orbitals, Figure 8c). As a result, the temperature-dependent VTF ion hopping only presents under the mismatch of coordination number and actual elemental ratio, reflecting the reasonable ion-molecule coordination contributes to ion mobility.[122]

Indeed, a slide-ring topological structure was proposed at the end of the 20th century for the mechanical enhancement of polymer gels. At the same time, ion transport modulation by molecular mobility and ion-molecule coordination interaction has been reported in recent years.[113] In bulk state, thermally activated ion hopping dominates, resulting in slow responsiveness and molecular relaxation according to time-temperature equivalence. Notably, this slide-ring supramolecular system is capable of quasi-solvent/vehicle ion transport rather than ion hopping by utilizing the sliding motion of rings threaded on crosslinked skeletons, and the solvent-independent ion transport mechanism indicates the negligible influence of environmental changes on ionic mobility. Accordingly, constructing a slide-ring crosslinked structure is a strategy to decouple the competition between device responsivity and stability.

3.3.2. Proton Transport in the Hydrogel Network

Hydrogen bonding is pervasive in both biological and chemical systems, serving as a powerful crosslinking effect for constructing topological structures (dual-network hydrogels) through self-assembly.[86,144,145] Crucially, densely oriented hydrogen bond arrangement is essential for the ion-dominant transport (especially proton transport) mechanism for establishing efficient and stable signaling in bioelectronics. In this section, we elaborate on the thermally activated proton transport mechanism from the energy perspective and provide an understanding of hydrogen/coordination bond exchange processes, followed by expounding the proton-dominant sensing mechanism in a hydrogen bond-crosslinked network.

Owing to the same Nernst potential of H^+ and OH^-, electrophysiological discrimination between H^+ and OH^- is tough, yet the proton transport can be described as Equation (1), whereas the E_a equals the binding energy of hydrogen bonds (1–50 kJ mol^{-1}) in this case (detailed information can be seen in the scientific literature[145]). As mentioned before, proton transport involves the hopping or tunneling of a proton from one molecule to the next through coordination bond exchange, leaving a negatively charged hydroxide ion (OH^-) as the 'proton hole'.[146] Similar to electrons, the energy level of protons as charge carriers presents a 'valence band' (bonded with H_2O) and a 'conduction band' (fluctuation of hydrogen bonds) when the protons are thermally activated. Nevertheless, unlike electrons, protons are not delocalized along the conduction band, yet segregated by potential barriers between the adjacent atoms/molecules (**Figure 9a**).[147] According to the hydration level in crosslinked structure and Gibbs Helmholtz equation, we can derive the proton mobility[146] (Equation 5) and the energy required to form an H^+/OH^- pair[148] (Equation 6) in a hydrogel system:

$$\sigma = kH^d \tag{5}$$

$$E = -k_B T \ln K_w \tag{6}$$

where H is the water content in hydrogel, k, and d represent the proportionality factor and critical exponent. In addition, K_w is the ion product constant of water, E denotes the bandgap and equals 0.83 eV (for other molecules that can produce protons, there exist distinct values of E[149,150]). Compared with covalent and ionic bonds, the binding energy of hydrogen bonds is relatively low, indicating the increased flexibility and ionic mobility in hydrogen-bonded topological supramolecules. The coordination bond exchange-induced proton transport can be divided

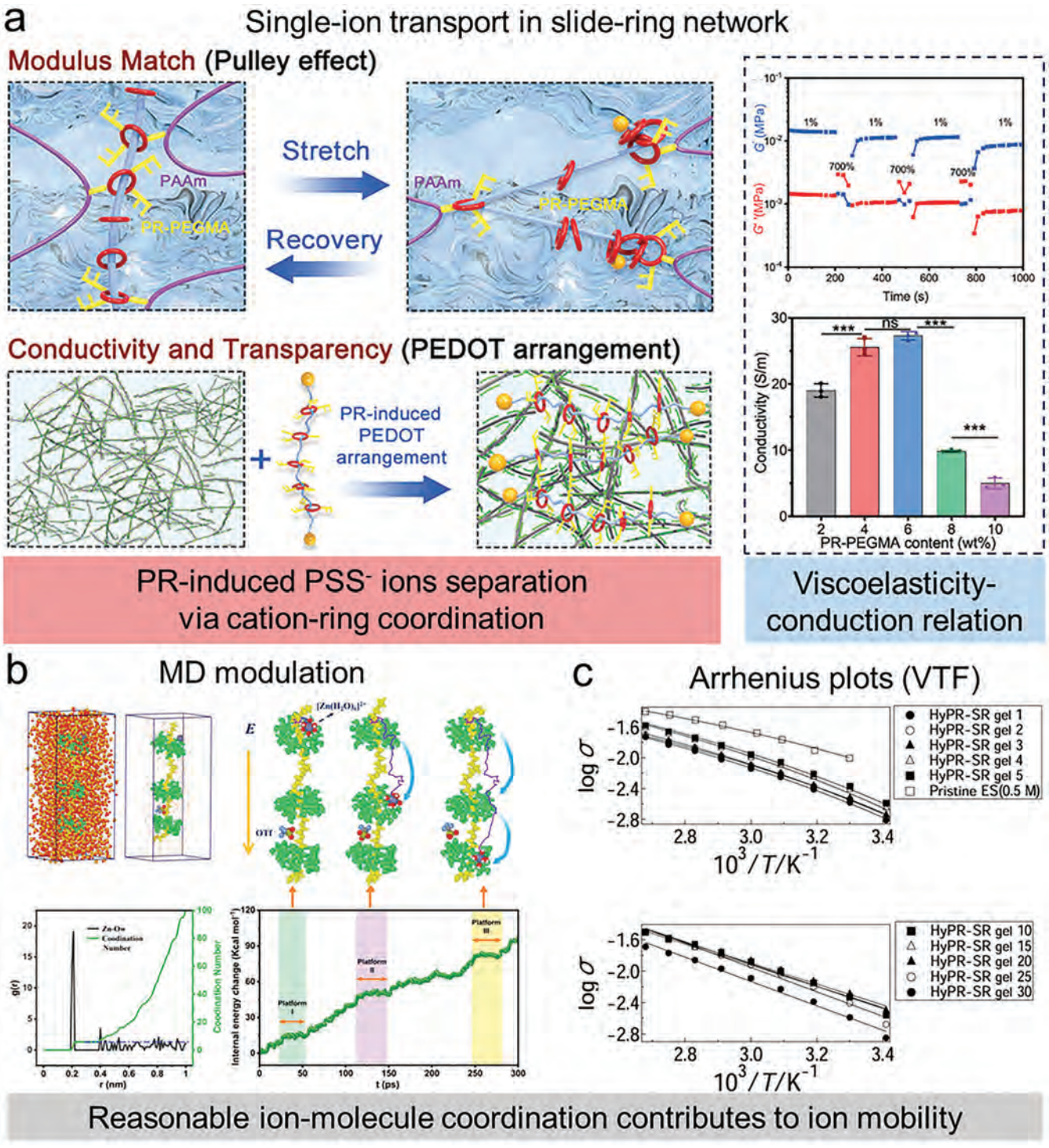

Figure 8. a) Single-ion transport in the slide-ring network via cation-ring coordination. The content of PR-based molecules can modulate the viscoelasticity and ion conductivity of the gels.[134] Reproduced with permission. Copyright 2023, Wiley-VCH GmbH; b) MD modulation, confirming the presence of single-ion transport. Reproduced with permission. Copyright 2023, Wiley-VCH GmbH; c) Arrhenius plots (VTF mode), indicating the rational ratio of cation/ligand is conducive to ion mobility. Reproduced with permission. Copyright 2017, Elsevier.

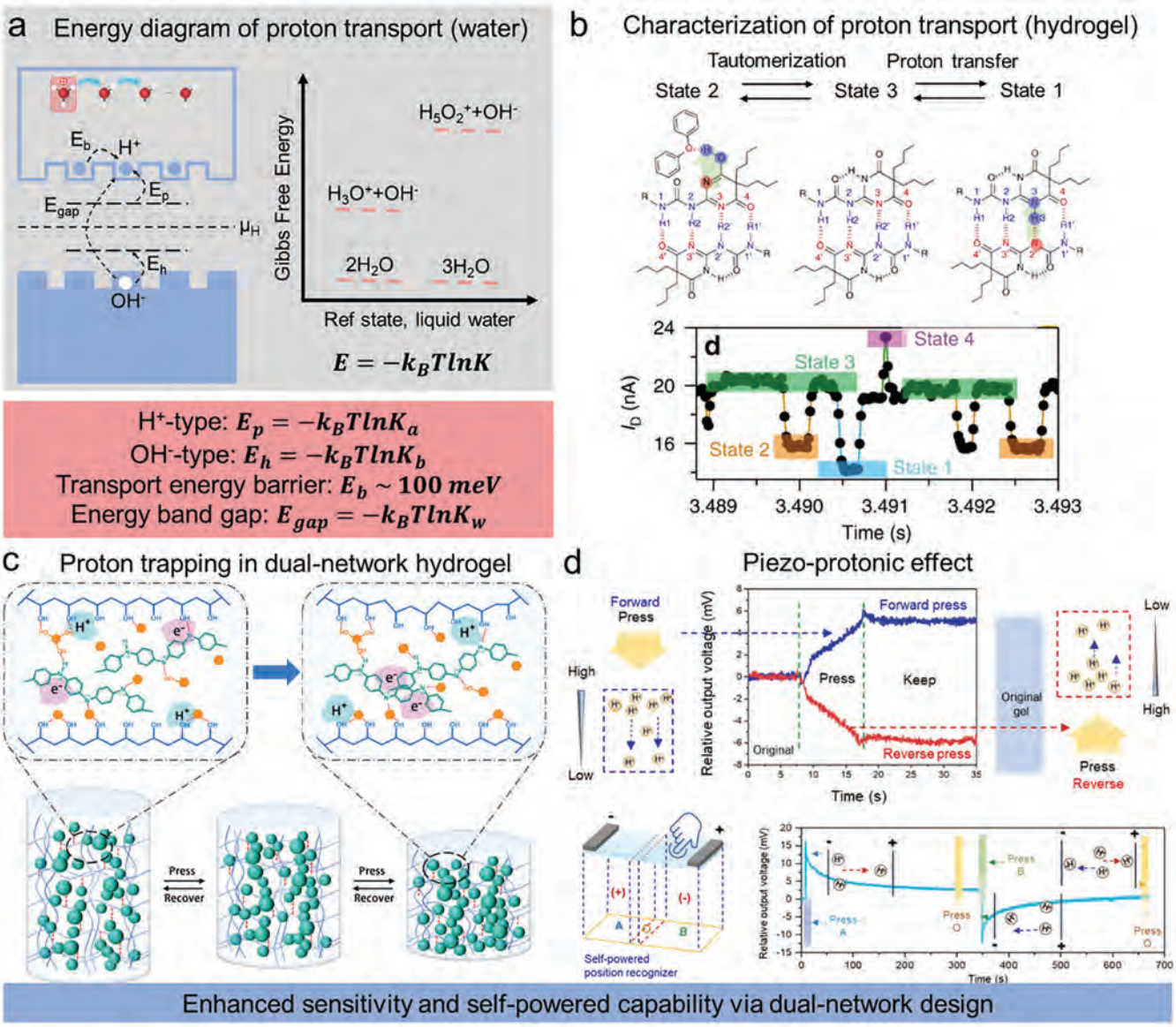

Figure 9. a) Energy diagram of proton transport (K_a/K_b: ionization equilibrium constant of Lewis acid/base).[147,154] Reproduced with permission. Copyright 2024, American Chemical Society; b) STM testing to characterize proton transport in the tetra-hydrogen bonding molecular system.[153] Reproduced with permission. Copyright 2018, Springer Nature; c) Proton trapping in the dual-network hydrogel.[155] Reproduced with permission. Copyright 2024, Elsevier; d) Piezo-protonic effect and self-powered sensors.[71] Reproduced with permission. Copyright 2022, Elsevier.

into three different processes (the vibrational motion dynamics of the hydrogen bonds, hydrogen atom or proton transfer reactions, and forming/breaking of hydrogen bonds), in which fundamental incidents can occur within an ultrafast period, ranging from femtoseconds to picoseconds.[140] Experimentally, ultrafast vibrational spectroscopy is utilized to detect the vibration of hydrogen bonds,[151] and hydrogen atom/proton reactions can be characterized by scanning tunneling microscopy (STM), illustrated in Figure 9b.[152] Furthermore, intramolecular and intermolecular proton hopping can be described by Femtosecond probing the electrical signals in solid-state device platforms (e.g., the ureidopyrimidinone (UPy) tetra-hydrogen bonding unit as the conduction layer and 2 graphene nanosheets as the electrode).[153] Combining the thermodynamic activity of protons and the characterization of these three fundamental physical processes, we can determine the proton transport mechanisms of the material and then design the appropriate applications based on such properties.

In hydrogel sensors with proton-dominant transport, the topological supramolecular structure is the critical index determining crosslinking density and arrangement of hydrogen bonding, thus affecting mechanical properties and conduction mechanisms. As mentioned in section 2.1, dual-network design, freeze-thaw, and sol-gel strategies endow hydrogels with anti-freezing and anti-swelling properties, which, in terms of strain sensors, avoid errors due to temperature and humidity variations,

respectively.[52,64,67] Additionally, the breakup and reassembly of hydrogen bonds during mechanical stretching can be modulated by alternately arranging soft/rigid segments.[156] Detailly, one of the segments possessing plentiful crosslinking sites (e.g., hydroxyl groups) is utilized for increasing hydrogen-bonded density, while another polymer network with hydrophilicity blocks between the former molecules, trapping protons for the enhancement of strain-sensitivity (Figure 9c).[121,155] Proposed by Chen et al., the PANI network was constructed between PVA molecules trapping protons by electrostatic interaction, leading to disruption of Grotthuss transport (confirmed by the relatively higher Ea: 0.17 eV).[121] Due to the rigidity differences between PVA and PANI, the dynamic hydrogen bonds serving as proton-transport channels were easily fractured under stretching, resulting in superior device sensitivity (GF = 24.6). A similar mechanism can also be found in soft/rigid molecular systems combined with flexible polymer and 2D materials. In this case, proton transport in intermolecular hydrogen bonds is controlled by changes in the interlayer spacing of nanosheets.[157,158] Additionally, benefiting from dynamic hydrogen-bonded TCNs, unidirectional proton transport can be realized by water/proton content-gradient topological structure design, endowing hydrogels with strain-induced self-powered/self-spiking properties in which the electricity is not derived from thermoelectricity, piezoelectricity, and triboelectricity (Figure 9d).[71,159]

Proton transport in hydrogels is an intriguing physical property that can be modulated by reconfiguration of dynamic hydrogen bonds in TCNs, thus leading to proton transport/hydrogen bond-related device applications, such as molecular recognition and nucleic acid/peptide sequencing.[160,161] Only by putting these insights into the molecular design in TCNs, which establishes a strong correlation between structure and device performance, can practical application of bioelectronic devices be obtained.

4. Application progress of TCN-E for artificial tactile neuron

Inspired by the neuron networks of animal brains, neuromorphic devices have garnered considerable attention and have been under intensive development for applications in AI perception of robotics,[1,3,136] human-machine interaction,[162] and recovery of impaired cell/neuron systems.[163] Though ionic/molecular systems utilized in bioelectronics are complex, the purpose of device design is consistent (i.e., enhancing the sensitivity of mechanoreceptors and reconfigurable performance in synaptic devices). Specifically, the implantation of tactile perception and neuromorphic computing mainly depends on ion transport and molecular reconfiguration mechanisms in bioelectronics, allowing sensitive mechano-response and modulation in synaptic connection, respectively.[162] Nevertheless, the sensitivity enhancement in conventional bioelectronic devices generally leads to bad cyclic stability due to viscoelastic imbalance in covalently crosslinked structures. By topological molecular design, the ion gels with dynamic crosslinked structures are capable of multimodal switching and ensuring relative stability of sensing.[153,155] Here, we mainly focus on the application progress of bioelectronic devices with topological design for artificial tactile neurons from the perspective of addressed scientific/engineering problems, compared with conventional bioelectronic systems dominant by electronic transport.

4.1. Artificial Self-Powered Tactile Neuron

In tactile neuron systems of humans, ion channels in dermatocytes composed of Piezo1/Piezo2 proteins as subunits will open in response to specific mechanical stimuli, allowing positively charged ions to flow into postsynaptic neurons.[164] Correspondingly, tactile sensors act as the sensation organs and presynaptic neurons generating and outputting electrical pulses under stimuli. At the same time, the post-connected organic field effect transistors/memristors will play a role in postsynaptic neurons processing the afferent tactile signals (**Figure 10**). However, the nature of the external energy supply increases the integration difficulty for capacitive and resistive sensors. As the proton transport mechanism describes, concentration gradient-induced ionic migration endows hydrogels with self-powered capability.[157,159] Switching the ionic pumping stage and EDL formation can also be realized by repeating contact/release between the object and ionic tactile sensors, resulting in mechanical-electrical energy conversion. In this case, the self-powered devices must be flexible and stretchable for integration with neuromorphic computing devices. Meanwhile, to achieve recognition of weak tactile signals, high energy conversion efficiency is prominent, mainly related to the mechanical sensitivity and ion transport of self-powered devices. To this end, topological ion gels have recently been used in flexible self-powered sensors to enhance output performance and sensitivity.

The first ion-gel-based self-powered strain sensor was proposed by Ye et al., which was fabricated by electrostatic spinning of ferroelectric/ion-liquid composites, with output voltage and current density of up to 45 V and 49 μA cm^{-2}, respectively.[166] The interfacial optimization and impedance matching of self-powered tactile sensors significantly enhance mechanical-electrical conversion efficiency and energy density. Various studies have pointed out that diminishing the internal resistance of flexible power devices by compositing with conductive nanofillers can improve the output performance.[167] Additionally, as reported by Xu et al., PVA-based ionic hydrogel was encapsulated by polydimethylsiloxane (PDMS) to form a semi-spherical microstructure, possessing superior output performance as the open-circuit voltage (V_{oc}) and short-circuit current (I_{sc}) were up to 150 V and 15 μA, respectively, under 10 MΩ loading (**Figure 11a**).[168] Furthermore, benefiting from the reconfigurability of TCNs, homogenous microstructure arrays of the ion gels can be easily achieved by sol-gel transition, realizing concentration of contact stress and interfacial conduction stability between the dielectric layer and ion transport layer (Figure 11b). For instance, Ke et al. fabricated high self-powered performance Al/PDMS microneedle sensors with the V_{oc} and I_{sc} of 167 V and 129.3 μA, respectively, which possessed higher stress-sensitivity (1.03 V N^{-1} and ≈3.11 V kPa^{-1}) than traditional tactile sensors (0.18–0.414 V N^{-1} and 0.013–0.29 V kPa^{-1})[169] at an area of 30 cm^2; Guo's group proposed a new strategy for e-skin design: through constructing topological interlinks between contact layer and microarrays, the tactile sensors can ensure the sensing stability under 1000 cycles (Figure 11c).[170] Despite facile

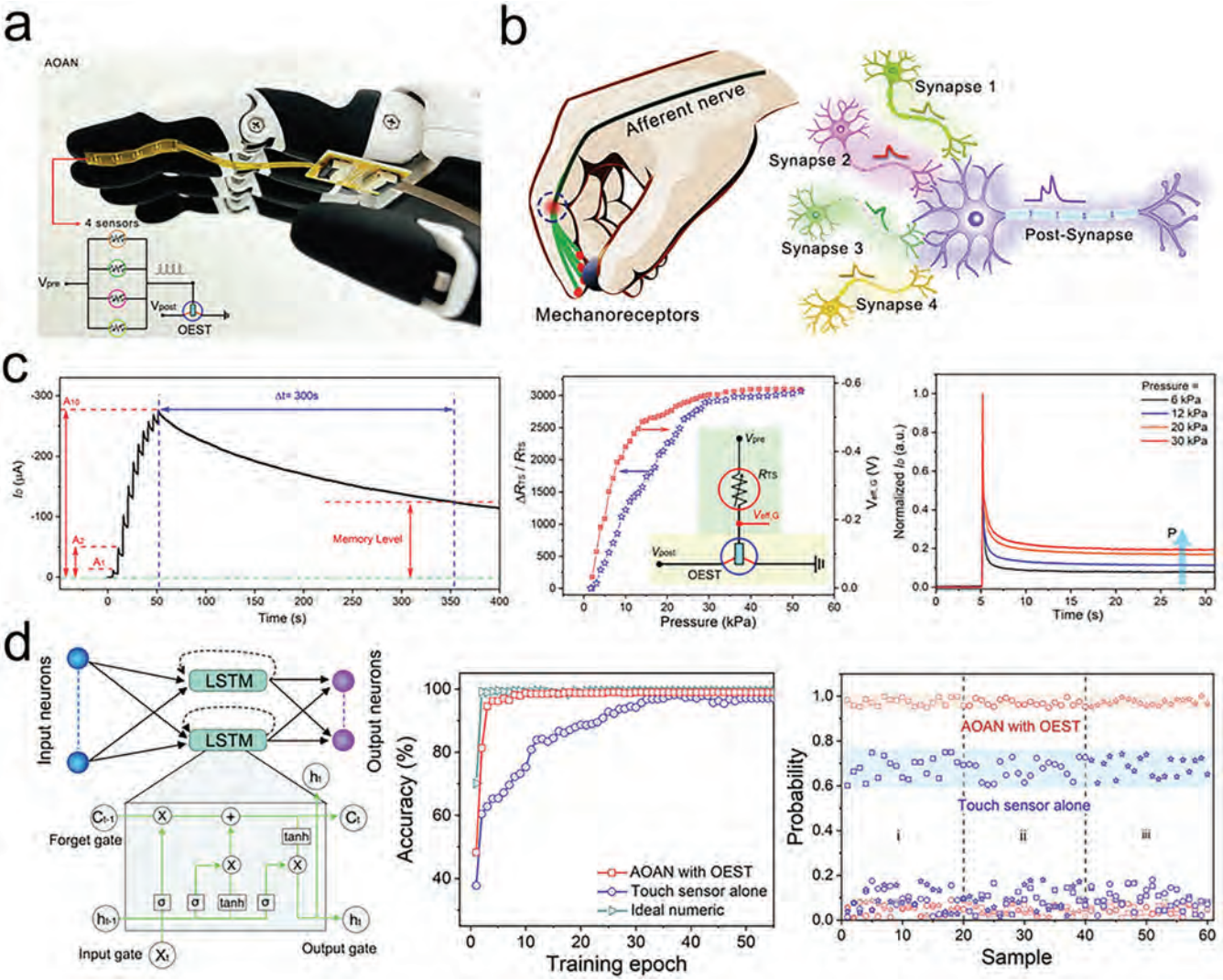

Figure 10. a) Artificial tactile neurons with four pre-synaptic sensors and one post-synaptic device; b) Illustration of the biological structure; c) Performance of synaptic devices. Memory levels increased with the raising pressures; d) Artificial neuromorphic network (ANN) for tactile perception, physical grabbing, and material recognition.[165] Reproduced with permission. Copyright 2024, Springer Nature.

microstructure processing, topological crosslinking design can endow multimodal sensing through ion transport-induced weak-strong structural conversion. Zhou et al. fabricated a bilayer gradient hydrogel by stacking Zn^{2+} and Fe^{3+} based ion gels, and ion diffusions of Zn^{2+} and Fe^{3+} were present under osmotic pressure to form an intermediate zone (Zn^{2+}/Fe^{3+}).[171] Due to the different coordination binding strengths of Fe^{3+} and Zn^{2+}, ionic tactile sensors with three ionic zones possessed regional viscoelasticity and high sensitivity (3.31 kPa^{-1}, 0–2 kPa), achieving the perception of light vibrations (e.g., feather) and binary information encryption. The self-powered tactile sensors can be integrated with memristors/capacitors based on ion gels to process the afferent tactile signals (Figure 11b). By topological molecular design, the postsynaptic transistors can reconfigure under external stimuli, modulating the synaptic weights for better machine-learning results and accurate tactile perception.[46] All these advances in material design paved the way for realizing fine-grained stress sensing of the ion gels (e.g., vertical and horizontal stress perception), which aimed at recognizing different objects according to their roughness, boosting the evolution of tactile neuromorphic devices. However, the developed self-powered tactile sensors can be adaptive to skin-friendly wearable applications but are still unfeasible for bio-implantation, hindered by the non-biocompatibility of chemical crosslinking surfaces.

4.2. Artificial Self-Healable Tactile Neuron

Recently, topological hydrogels with excellent biocompatibility have received tremendous attention for developing self-healable tactile sensors. The biocompatibility of synthetic polymers can be evaluated based on several key aspects: degradation properties, compatibility with cells, and blood compatibility. Different biopolymers exhibit unique applications depending on their

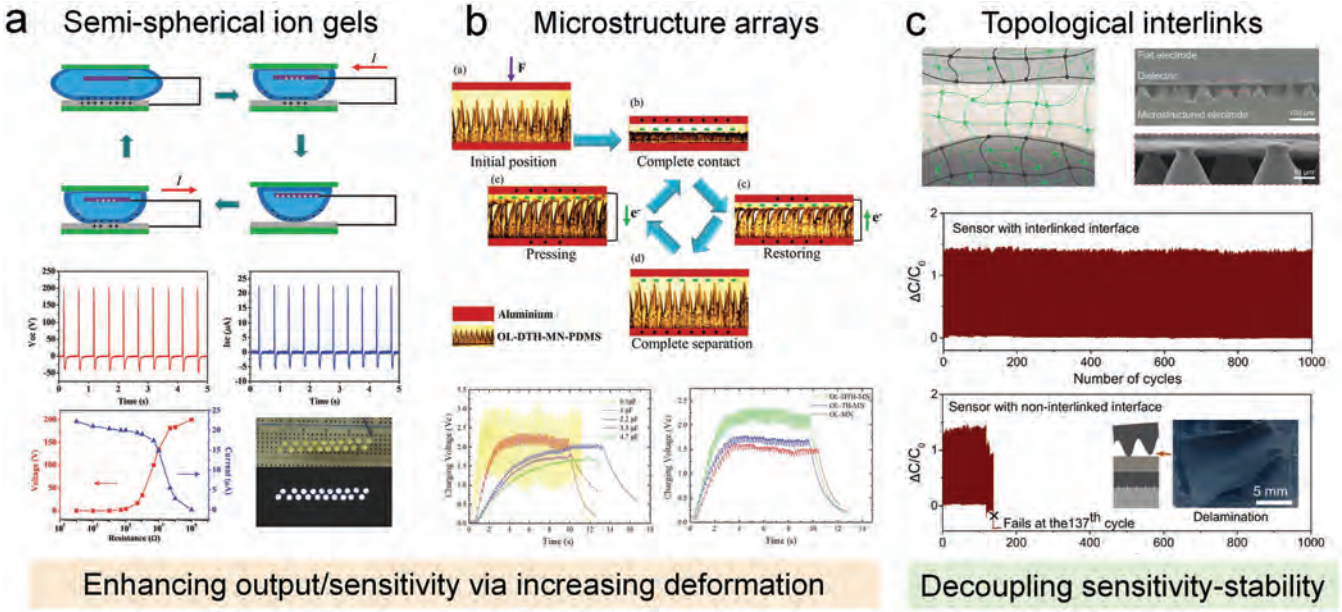

Figure 11. Recent advances in self-powered tactile sensors. a) Semi-spherical PVA/PDMS ion gels with the output performance.[168] Reproduced with permission. Copyright 2016, Wiley-VCH GmbH; b) Microstructure arrays based on PDMS with the output performance while charging the capacitors with different capacitances.[169] Reproduced with permission. Copyright 2020, Wiley-VCH GmbH; c) Topological crosslinking strategy enhancing interfacial stability.[170] Reproduced with permission. Copyright 2022, Springer Nature.

mechanical properties and biocompatibility. For instance, PVA (partially biodegradable) and cellulose (biodegradable into glucose) demonstrate good compatibility with soft tissues and low platelet adhesion, making them well-suited for applications emphasizing soft tissue compatibility and hydrogel characteristics, such as wound dressings or drug delivery systems.[172] In contrast, PAA and PAM, which are not easily degradable, may contain impurities with cytotoxicity and exhibit low blood compatibility. These materials often require pH control and chemical modifications for further applications.[173] PLA (polylactic, biodegradable into lactic acid) typically requires surface hydrophilic modification to improve cellular compatibility. Its tendency to activate platelets, combined with high mechanical strength and rigidity, makes it ideal for complex tissue repair, such as bone scaffolds and surgical sutures.[174] PEDOT:PSS, while not fully biodegradable, offers high electrical conductivity and can withstand minor mechanical deformation, making it suitable for implantable biosensors, neuronal repair, and cardiac repair applications.[175]

Self-healing of polymers is usually achieved through the flow of amorphous polymers at temperatures higher than T_g and the rearrangement of reversible bonds, including dynamic covalent bonding and physical interactions.[41] Compared with dynamic covalent crosslinking based on the thermodynamic equilibrium between the breakup and reconnection of the crosslinking bonds, TCNs with dynamic physical interactions can be desirable to enable autonomous self-healing capability without external stimuli (**Figure 12a**).[10,38,176] In this case, TCN-based tactile sensors can possess high self-healing efficiency under ambient temperature or even extreme conditions.[177] Additionally, topological hydrogels can reversible reconfiguration under temperature changes, achieving tactile sensation and self-healing capabilities of sensors like human skin. For humans, injuries in which peripheral nerves are wholly severed, such as deep cuts from accidents, can be challenging to treat.[178] By leveraging the tactile sensing capability and biocompatibility of topological hydrogels, the fabricated sensors can be implanted in mammals, replacing the damaged nerves to conduct bioelectric signals and boost neuronal repair.

However, there are still problems like interfacial mechanical mismatch, transport decoupling of tactile signals to brain neurons, and imprecise reconstruction of neuronal conduction across the lesion site after injury. Here are the recent strategies to combat these handicaps. First, modulating the ratio of polar molecules to crosslinked molecules is vital to balance self-healing and adhesion capabilities.[176] In addition, Liu reported a mechanical-interlocking effect between the contacting layer (elastomer) and the sensing layer (hydrogel) due to the introduction of branched-topological coupling agents, boosting the interfacial mechanical stability of the sensors (Figure 12b).[179] Second, Kang et al. reported an artificial skin consisting of collagen and fibrin with a PU-based substrate, which facilitated layer-by-layer skin regeneration, and the hydrogel-coated surface minimizes foreign body reactions to realize an effective long-term nerve stimulation while replacing the permanently damaged mechanoreceptors with a tactile sensor (Figure 12c).[180] Third, biomaterials containing nerve repair nutrients are encapsulated with brush polymers to form topological hydrogels to achieve precise neuronal conduction and axal regeneration.[181] Besides, the dual-network hydrogels were utilized to replace the damaged tactile sensing nerves transporting signals and offering healing microenvironments (Figure 12d). All these results illustrate the great potential application of TCN-E in biological and medical fields.

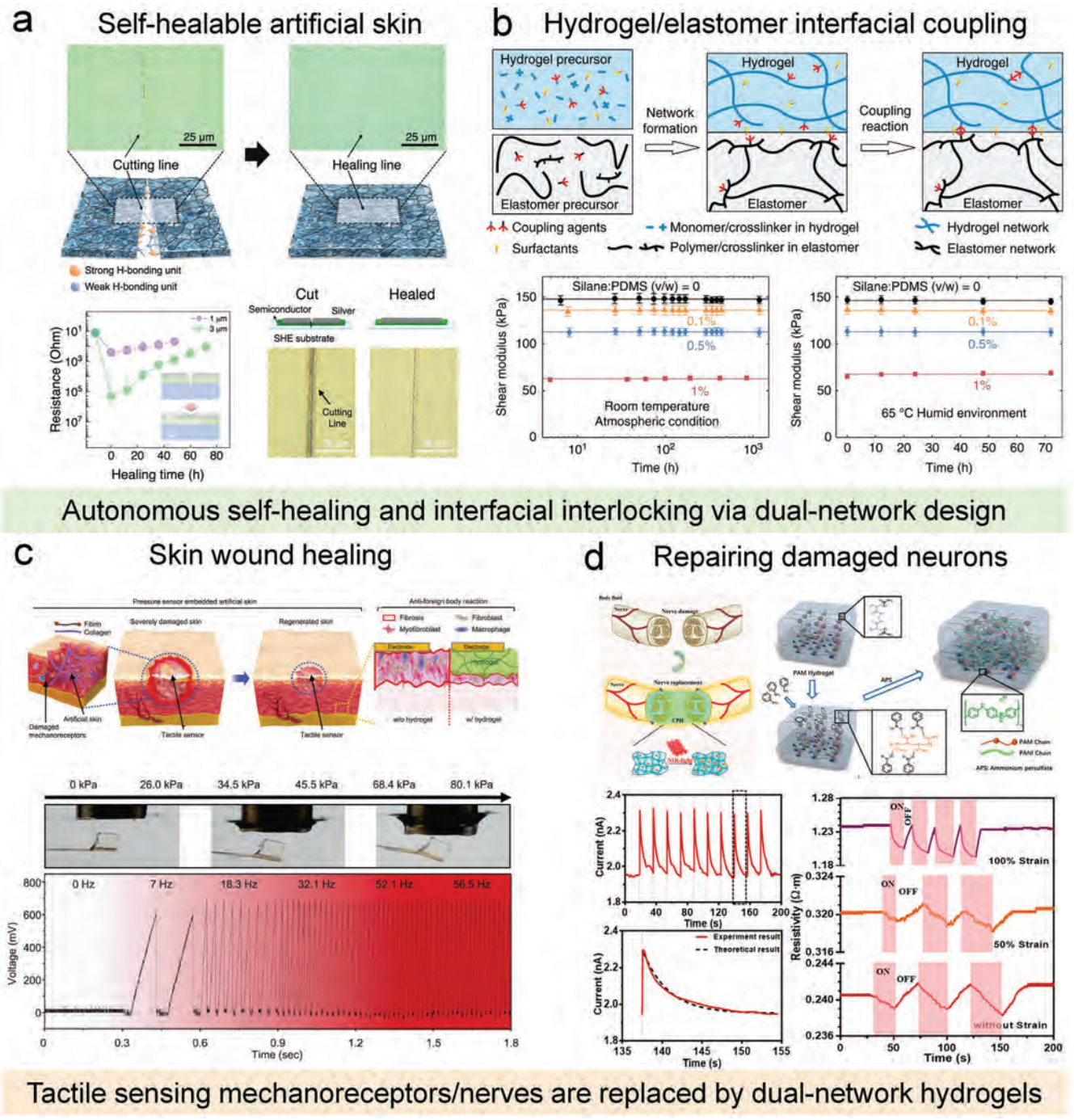

Figure 12. a) Artificial self-healable skin with the performance comparison before/after cutting.[38] Reproduced with permission. Copyright 2022, Springer Nature; b) Interfacial coupling between PDMS and hydrogel. Reproduced with permission.[179] Copyright 2020, American Chemical Society; c) Demonstration of skin wound healing and the strain stimulation-response under different frequencies.[180] Reproduced with permission. Copyright 2024, Springer Nature; d) Illustration of repairing damaged neurons by bridging dual-network hydrogels and the sensing performance of hydrogels.[178] Reproduced with permission. Copyright 2020, American Chemical Society.

4.3. Artificial Multimodal-Sensing Tactile Neuron

Tactile perception can be classified into two main subsystems: one for temperature, detected by free nerve endings and Krause end bulbs in the skin, and one for mechanical stimuli, detected by Meissner's corpuscles, Merkel's discs, Pacinian corpuscle, and Ruffini endings.[182] Realizing realistic tactile reproduction requires a feedback interface that provides as much multidimensional information as possible. The construction of TCNs can endow the ion gels with the ability to respond to the environment

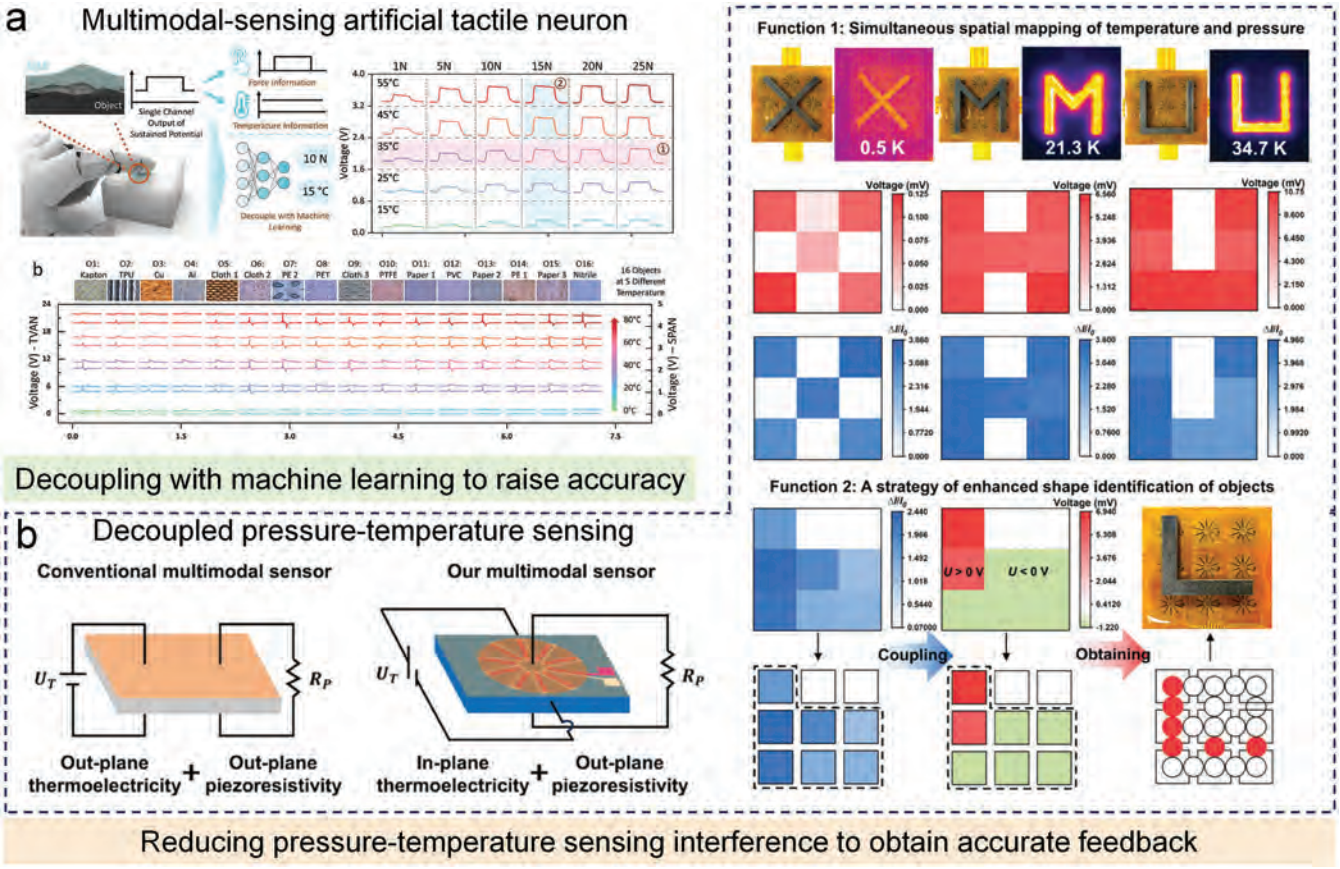

Figure 13. a) Illustration of multimodal sensing and feature fusion for machine learning.[184] Reproduced with permission. Copyright 2024, Wiley-VCH GmbH; b) Demonstration of the decoupled pressure-temperature sensing and 2 functions of the multimodal sensor.[185] Reproduced with permission. Copyright 2023, Wiley-VCH GmbH.

(i.e., temperature in particular) in addition to the mechanical response. Combined with the rational surface structure design and neural network algorithms, the TCN-based artificial tactile neuron can realize multimodal sensing and perform complex tasks[183]. For example, Guo et al. prepared and designed artificial tactile neurons based on PVA/PAA/Li^+ dual-network hydrogels with textile/pressure/temperature sensing capabilities and feature fusion for machine learning to achieve material recognition, healthcare monitoring, and physical grasping (**Figure 13a**).[184]

To enhance the accuracy, in addition to algorithmic optimization, it is vital to ensure stability while the sensors are being squeezed/stretched and increase the differentiation of tactile signal waveforms. Besides, as for the layer-by-layer (mechanoreceptors/temperature sensors/electrodes/substrates) artificial skin system, the main problems are interfacial mismatch and lack of stretchability under miniaturization.[186] As mentioned, the ion gels with TCNs can be easily printed and micro-structured for a highly integrated tactile perception system with enhanced interfacial adhesion and mechanical stability. Zhang et al. reported a cellulose nanofiber-based PAA@Fe^{3+} topological supramolecular hydrogel system with good adhesion strength up to 90 N m^{-1} before UV radiation.[187] Additionally, there is still interference between temperature and stress sensing while these two functional layers are integrated. For example, Wang et al. utilized an insulating PI layer to separate the in-plane thermoelectric generator and out-plane micro-cone pressure sensor to decouple temperature-pressure sensing fully. The flexible multimodal tactile sensor possessed remarkable temperature sensitivity (281.46 μV K^{-1}) and can detect a temperature difference as small as 0.1 K, with a short response/recovery time of 0.78 s/1.65 s[185] (Figure 13b). With temperature sensing in artificial tactile neurons, accurate feedback can be obtained by processing the afferent electrical signals, increasing the similarity between real tactile feelings and the machine learning results. These rich interactions and multisensory feedback make bringing the virtual world closer to reality possible, allowing users a more immersive experience.[182]

5. Conclusion and Outlook

In this review, we highlighted the recent advances in bioelectronics with TCN design and the application progress for artificial tactile neurons, which includes the assembly methods to the efforts toward the development of a stable, sensitive, reconfigurable human-like skin system with self-powered and self-healing capabilities. Additionally, we revealed the ion-dominant transport mechanism in TCNs, whose transport efficiency is closely related to the molecular conformation (single-ion transport in slide-ring

structure and proton transport in the hydrogen-bonded network), which is distinct from the traditional electron-dominant conjugated molecular system. In this case, artificial neuromorphic devices with ion channels are suitable for implanting in human cell environments for biological and medical research and applications. At the same time, there is a need for more professional insights and in-depth research to conquer scientific issues. Here, combined with the recent advances in artificial tactile neuromorphic devices, we mainly focus on the addressed scientific/engineering problems by topological crosslinking structure design: 1) decouple competing effects using multiple molecular building blocks to meet complex requirements; 2) modulate conductance by molecular reconfiguration through external-stimuli, enhancing the sensing range of the sensors and endowing multimodal-sensing capabilities; 3) optimize interfaces of the layer-by-layer artificial tactile neuron by combining similar polymers in conductor, semiconductor, and dielectric, serving as electrodes, channels and substrates, respectively.

From the engineering perspective, IC circuit painting and micro-structuring all require the preparation of gel-ink (sol-gel transition), and polymers with low T_g such as PVA, PAM, PAA, and PEDOT:PSS is suitable to be utilized as the main skeleton of ion gels. Freeze-thaw cycling can be used post-processing to endow the gel units with anti-freezing/anti-swelling capabilities for temperature/humidity sensing applications. Given the single-molecular limitations (e.g., PVA is not conductive and PEDOT:PSS is mechanically unstable), topological molecular combination is a compromising solution. Specifically, to decouple stretchability and conductivity, PVA/CD/proton-carrier mixed ion gel systems with slide-ring topology (host-guest reaction) can be a terrific choice, as the CD rings will enhance chain-motion and proton-anion separation will present via ring's dynamic hydrogen bonding effect and spatial potential resistance effect. Afterward, to decouple sensitivity and stability, PVA/EA/Fe^{3+} hydrogel systems with PDMS encapsulation will be desirable as the hydrogel enables being reconfigured into stress-sensitive microunits, and EA-Fe^{3+} nanoclusters can simultaneously improve the cohesion of hydrogel and mechanical interlocking between PVA/PDMS phases, due to the branched conformation of nanoclusters. Two strategies have been proposed by Suo's group and Stephen's group to decouple reinforcement and toughness. For the former, the strategy is to prepare far more entangled hydrogels than crosslinked hydrogels by using small amounts of water, crosslinking agents, and initiators in the synthesis process.[188] The force-coupled reaction was present for the latter by introducing force-sensitive groups (mechanophores) into dual-network hydrogels. In contrast, hydrogels were stretched, causing the force-sensitive groups to open the rings, thus lengthening the polymer chain segments and the synchronous promotion of toughness and strength.[189] These strategies provided insights into engineering theory for TCNs, which can be applied to e-skin or artificial tactile neurons in the future.

Additionally, from the scientific/technical point of view, the characterization of ion/electron transport and sensor performance is significant. As mentioned in Chapter 3, the ion-hopping energy and ionic conductivity can be calculated by empirical formulas, and the direct detection of ion transporting and biosensing signals can be realized by the cascade of STM, ultrafast vibrational spectroscopy, and femtosecond-level probing. The research of ion transport mechanisms and molecular dynamics in TCNs provides new insights into the electrochemical doping mechanism and ionic-electronic coupling effect, which is conducive to understanding and optimizing the EDL process. Besides, the study on dynamic molecular interactions is significant for understanding the relation between molecular structures and mechanical/physical properties, providing theoretical basics in constructing artificial perception neurons with self-powered, self-healable, multimodal-sensing, and even more capabilities. Technical improvements, including combining 3D printing technology, multimode integration, and machine learning, are required to improve sensing/perception performance. Bioelectronics' ultimate goal- an artificial neuromorphic perception system- will need a revolutionary device architecture and an integrated systems approach that must be compatible with the semiconductor industry.

Compared to systems with only conjugated molecules, bioelectronics with TCN design possessed certain advantages in molecular flexibility, ion transport efficiency, and self-powered/self-healable/multimodal-sensing capabilities. Nevertheless, there are still challenges for practical applications: 1) the inhomogeneity problem of microarrays owing to the limited material choice for printing or molding; 2) enhancing environmental stability and durability of the miniaturized device arrays and ensure each unit can work individually and possessing uniform performance. 2) incorporate more tactile sensing modes like shear forces and torsional forces; 4) bionic skin may have tactile sensing capabilities, but it is difficult to simultaneously realize temperature sensing, pressure distribution detection, and self-healing. Accordingly, the viscoelastic modulation of crosslinked networks by introducing different topological molecules should be further investigated to solve technical issues like sensitivity and stability for practical application and establish viscoelasticity-related conductance mechanism (e.g., ionic transport or the efficient energy utilization mechanism in nature) toward a higher level of multifunctional biomimetic structure design. We believe that bioelectronics' topological crosslinking structure design and performance trade-offs will be the major driving direction of artificial tactile neuromorphic perception devices and systems.

Acknowledgements

This research was financially supported by a fellowship award from the Research Grants Council of the Hong Kong Special Administrative Region, China (CityU RFS2021–1S04) and the State Key Laboratory of Terahertz and Millimeter Waves (City University of Hong Kong).

Conflict of Interest

The authors declare no conflict of interest.

Keywords

artificial tactile neurons, bioelectronics, ion/electronic transport, topological crosslinked network

Received: October 29, 2024
Revised: December 30, 2024
Published online: February 4, 2025

[1] D. Lu, T. Liu, X. Meng, B. Luo, J. Yuan, Y. Liu, S. Zhang, C. Cai, C. Gao, J. Wang, S. Wang, S. Nie. *Adv. Mater.* **2023**, *35*, 2209117.
[2] K. Xia, J. Liu, W. Li, P. Jiao, Z. He, Y. Wei, F. Qu, Z. Xu, L. Wang, X. Ren, B. Wu, Y. Hong, *Nano Energy* **2023**, *105*, 107974.
[3] S. Chun, J.-S. Kim, Y. Yoo, Y. Choi, S. J. Jung, D. Jang, G. Lee, K.-I. Song, K. S. Nam, I. Youn. *Nat. Electron.* **2021**, *4*, 429.
[4] X. Li, F. R. Chen, Y. Lu. *Interdiscip. Mater.* **2024**, *3*, 835.
[5] S. Wang, J. Xu, W. Wang, G.-J. N. Wang, R. Rastak, F. Molina-Lopez, J. W. Chung, S. Niu, V. R. Feig, J. Lopez, T. Lei, S.-K. Kwon, Y. Kim, A. M. Foudeh, A. Ehrlich, A. Gasperini, Y. Yun, B. Murmann, J. B.-H Tok, Z. Bao, *Nature* **2018**, *555*, 83.
[6] A. Chortos, J. Liu, Z. Bao. *Nat. Mater.* **2016**, *15*, 937.
[7] A. N. Sokolov, M. E. Roberts, Z. Bao. *Mater. Today* **2009**, *12*, 12.
[8] J. Liu, B. Jiang, J. Ji, F. Cheng, C. Cai, Y. Fu. *Chem. Eng. J.* **2024**, *497*, 154672.
[9] E. Su, M. Yurtsever, O. Okay. *Macromolecules* **2019**, *52*, 3257.
[10] D. Liu, G. Yin, X. Le, T. Chen. *Polym. Chem.* **2022**, *13*, 1940.
[11] K. Ito. *Curr. Opin. Solid State Mater. Sci.* **2010**, *14*, 28.
[12] C.-A. Palma, J. Björk, F. Rao, D. Kühne, F. Klappenberger, J. V. Barth. *Nano Lett.* **2014**, *14*, 4461.
[13] W. Li, M. Cai, Y. Yao, Y. Huang, H. Wu, W. Wu, J. Wen, J. Wu. *J. Mater. Chem. A* **2024**, *12*, 23638.
[14] G. Wu, Y. Wang, Y. Shen, H. Zheng, Y. Zeng, C. Zhang, X. Zhang, S. Zhang, J. Zhang, Z. Yu. *Adv. Mater. Interfaces* **2023**, *10*, 2300262.
[15] Z. Zhang, L. Qian, B. Zhang, C. Ma, G. Zhang. *Angew. Chem.* **2024**, *63*, e202410335.
[16] J. Ye, H. Jin, Z. Zu, B. Yu, H. Xiang, M. Zhang. *Engineer. Sci.* **2023**, *22*, 815.
[17] F. Herbst, D. Döhler, P. Michael, W. H. Binder. *Macromol. Rapid Commun.* **2013**, *34*, 203.
[18] S. Chen, N. Mahmood, M. Beiner, W. H. Binder. *Angew. Chem.* **2015**, *127*, 10326.
[19] K. Zhang, X. Chen, Y. Xue, J. Lin, X. Liang, J. Zhang, J. Zhang, G. Chen, C. Cai, J. Liu. *Adv. Funct. Mater.* **2022**, *32*, 2111465.
[20] J. Feng, J. Allgaier, M. Kruteva, S. Förster, W. Pyckhout-Hintzen. *Front. Soft Matter* **2023**, *3*, 1221803.
[21] X. Lin, Y.-Y. Deng, Q. Zhang, D. Han, Q. Fu. *Macromolecules* **2023**, *56*, 1243.
[22] H. Meng, W. Ye, C. Wang, Z. Gao, B. Hu, C. Wang, *Carbohydr. Polym.* **2022**, *298*, 120145.
[23] Q. Wang, X. Ji, X. Liu, Y. Liu, J. Liang. *ACS Nano* **2022**, *16*, 12677.
[24] W. Li, H. Wu, Y. Huang, Y. Yao, Y. Hou, Q. Teng, M. Cai, J. Wu. *Angew. Chem., Int. Ed.* **2024**, *63*, e202408250.
[25] L. Hu, X. Zhu, C. Yang, M. Liu. *Angew. Chem., Int. Ed.* **2022**, *61*, e202114759.
[26] G. D. Goh, J. M. Lee, G. L. Goh, X. Huang, S. Lee, W. Y. Yeong. *Tissue Eng., Part A* **2023**, *29*, 20.
[27] A. Mikhaylov, A. Pimashkin, Y. Pigareva, S. Gerasimova, E. Gryaznov, S. Shchanikov, A. Zuev, M. Talanov, I. Lavrov, V. Demin. *Front. Neurosci.* **2020**, *14*, 358.
[28] S. Oh, J. Jekal, J. Liu, J. Kim, J. U. Park, T. Lee, K. I. Jang. *Adv. Funct. Mater.* **2024**, 2403562.
[29] F. Wang, Y. Xue, X. Chen, P. Zhang, L. Shan, Q. Duan, J. Xing, Y. Lan, B. Lu, J. Liu. *Adv. Funct. Mater.* **2024**, *34*, 2314471.
[30] F. Liu, X. Liu, H. Gu. *Macromol. Mater. Eng.* **2022**, *307*, 2100724.
[31] X. Fan, J. Geng, Y. Wang, H. Gu. *Polymer* **2022**, *246*, 124769.
[32] Y. Jiang, Z. Zhang, Y.-X. Wang, D. Li, C.-T. Coen, E. Hwaun, G. Chen, H.-C. Wu, D. Zhong, S. Niu, W. Wang, A. Saberi, J.-C. Lai, Y. Wu, Y. Wang, A. A. Trotsyuk, K. Y. Loh, C.-C. Shih, W. Xu, K. Liang, K. Zhang, Y. Bai, G. Gurusankar, W. Hu, W. Jia, Z. Cheng, R. H. Dauskardt, G. C. Gurtner, J. B.-H. Tok, K. Deisseroth, et al., *Science* **2022**, *375*, 1411.
[33] D. G. Mackanic, X. Yan, Q. Zhang, N. Matsuhisa, Z. Yu, Y. Jiang, T. Manika, J. Lopez, H. Yan, K. Liu, X. Chen, Y. Cui, Z. Bao. *Nat. Commun.* **2019**, *10*, 5384.
[34] Q. Lin, C. Ke. *Chem. Commun.* **2022**, *58*, 250.
[35] I. Pochorovski, H. Wang, J. I. Feldblyum, X. Zhang, A. L. Antaris, Z. Bao, *J. Am. Chem. Soc.* **2015**, *137*, 4328.
[36] T. Z. Gao, Z. Sun, X. Yan, H.-C. Wu, H. Yan, Z. Bao. *Small* **2020**, *16*, 2000923.
[37] A. Chortos, I. Pochorovski, P. Lin, G. Pitner, X. Yan, T. Z. Gao, J. W. To, T. Lei, J. W. Will III, H.-S. P. Wong. *ACS Nano* **2017**, *11*, 5660.
[38] N. T. P. Vo, T. U. Nam, M. W. Jeong, J. S. Kim, K. H. Jung, Y. Lee, G. Ma, X. Gu, J. B. H. Tok, T. I. Lee, Z. Bao, J. Y. Oh. *Nat. Commun.* **2024**, *15*, 3433.
[39] J. Lopez, Z. Chen, C. Wang, S. C. Andrews, Y. Cui, Z. Bao. *ACS Appl. Mater. Interfaces* **2016**, *8*, 2318.
[40] C. Zhang, C. Wang, C. Li, T. Zhang, Y. Jiang, X. Cheng, K. Wang, C. Ma, Y. Li. *Appl. Phys. Rev.* **2024**, *11*.
[41] H. Wang, X.-Q. Xie, Y. Peng, J. Li, C.-S. Liu. *J. Colloid Interface Sci.* **2021**, *590*, 103.
[42] A. Nawaz, Q. Liu, W. L. Leong, K. E. Fairfull-Smith, P. Sonar. *Adv. Mater.* **2021**, *33*, 2101874.
[43] J. Rivnay, S. Inal, A. Salleo, R. M. Owens, M. Berggren, G. G. Malliaras, *Nat. Rev. Mater.* **2018**, *3*, 1.
[44] A. Marks, S. Griggs, N. Gasparini, M. Moser. *Adv. Mater. Interfaces* **2022**, *9*, 2102039.
[45] Y. Zhang, L. Liu, B. Tu, B. Cui, J. Guo, X. Zhao, J. Wang, Y. Yan. *Nat. Commun.* **2023**, *14*, 247.
[46] H. Tian, C. Wang, Y. Chen, L. Zheng, H. Jing, L. Xu, X. Wang, Y. Liu, J. Hao, *Sci. Adv.* **2023**, *9*, eadd6950.
[47] J. Song, H. Liu, Z. Zhao, P. Lin, F. Yan. *Adv. Mater.* **2024**, *36*, 2300034.
[48] T. S. Rao, S. Kundu, B. Bannur, S. J. George, G. U. Kulkarni, *Nanoscale* **2023**, *15*, 7450.
[49] J. Ajayan, P. Mohankumar, R. Mathew, L. R. Thoutam, B. K. Kaushik, D. Nirmal, *IEEE Trans. Electron Devices* **2023**, *70*, 3401.
[50] H. Sun, C. P. Kabb, M. B. Sims, B. S. Sumerlin. *Prog. Polym. Sci.* **2019**, *89*, 61.
[51] T. Mutai, S. Takamizawa. *J. Photochem. Photobiol., C* **2022**, *51*, 100479.
[52] J. M. Dodda, M. G. Azar, P. Bělský, M. Šlouf, A. Brož, L. Bačáková, J. Kadlec, T. Remiš. *Cellulose* **2022**, *29*, 6697.
[53] L. Lin, L. Zhang, Y. Guo. *Mater. Res. Express* **2018**, *5*, 015702.
[54] N. Wang, X. Yang, X. Zhang. *Nat. Commun.* **2023**, *14*, 814.
[55] G. C. Luque, M. L. Picchio, A. P. S. Martins, A. Dominguez-Alfaro, L. C. Tomé, D. Mecerreyes, R. J. Minari. *Macromol. Biosci.* **2020**, *20*, 2000119.
[56] W. Niu, Q. Tian, Z. Liu, X. Liu. *Adv. Mater.* **2023**, *35*, 2304157.
[57] H. He, H. Li, A. Pu, W. Li, K. Ban, L. Xu. *Nat. Commun.* **2023**, *14*, 759.
[58] X. Fan, L. Zhao, Q. Ling, H. Gu. *Industr. Engineer. Chem. Res.* **2022**, *61*, 3620.
[59] P. Du, J. Wang, Y.-I. Hsu, H. Uyama. *ACS Appl. Mater. Interfaces* **2023**, *15*, 23711.
[60] A. Giovagnoli, G. D'Altri, L. Yeasmin, V. Di Matteo, S. Scurti, M. F. Di Filippo, I. Gualandi, M. C. Cassani, D. Caretti, S. Panzavolta, M. L. Focarete, M. Rea, B. Ballarin. *Gels* **2024**, *10*, 458,
[61] Y. Xue, X. Chen, F. Wang, J. Lin, J. Liu. *Adv. Mater.* **2023**, *35*, 2304095,
[62] J. H. Choi, J. S. Lee, D. H. Yang, H. Nah, S. J. Min, S. Y. Lee, J. H. Yoo, H. J. Chun, H.-J. Moon, Y. K. Hong. *ACS Omega* **2023**, *8*, 44076.
[63] Y. Deng, M. Yang, G. Xiao, X. Jiang. *Int. J. Biol. Macromol.* **2024**, *257*, 128566.
[64] J. Lu, J. Gu, O. Hu, Y. Fu, D. Ye, X. Zhang, Y. Zheng, L. Hou, H. Liu, X. Jiang. *J. Mater. Chem. A* **2021**, *9*, 18406.
[65] Z. Guo, Z. Wang, W. Pan. *Micro Nano Lett.* **2023**, *18*, e12181.
[66] S. Feng, J. Guo, F. Guan, J. Sun, X. Song, J. He, Q. Yang. *Colloids Surf., A* **2023**, *676*, 132141.
[67] Y. Li, Y. Gu, S. Qian, S. Zheng, Y. Pang, L. Wang, B. Liu, S. Liu, Q. Zhao. *Nano Res.* **2024**, *17*, 5479.

[68] Q. Chen, Z.-R. Yang, S. Du, S. Chen, L. Zhang, J. Zhu. *Int. J. Biol. Macromol.* **2024**, *257*, 128636.
[69] J. Yan, J. P. K. Armstrong, F. Scarpa, A. W. Perriman. *Adv. Mater.* **2024**, *36*, 2403937.
[70] A. Roy, S. Zenker, S. Jain, R. Afshari, Y. Oz, Y. Zheng, N. Annabi. *Adv. Mater.* **2024**, *36*, 2404225.
[71] X. Pan, Q. Wang, D. Benetti, Y. Ni, F. Rosei. *Nano Energy* **2022**, *103*, 107718.
[72] W. Zhu, Y. Zhang, S. Huang, L. Geng, J. Wu, G. Mao, X. Peng, Y. Cheng. *Chem. Eng. J.* **2024**, *497*, 154409.
[73] X. Pan, Y. Li, W. Pang, Y. Xue, Z. Wang, C. Jiang, C. Shen, Q. Liu, L. Liu. *Int. J. Pharm.* **2022**, *617*, 121612.
[74] C. Wang, Y. Jiang, Q. Ji, Y. Xing, X. Ma. *J. Cleaner Prod.* **2024**, *435*, 140503.
[75] Y. Hui, R. Liu, T. Sun, L. Li, Y. Gong, Z. Xiao, A. Xu, X. Wei. *Macromolecules* **2024**, *57*, 4737.
[76] H. Zhang, N. Tang, X. Yu, Z. Guo, Z. Liu, X. Sun, M.-H. Li, J. Hu. *Chem. Eng. J.* **2022**, *430*, 132779.
[77] L. Chen, J. Shao, Q. Yu, S. Wang. *J. Dispersion Sci. Technol.* **2022**, *43*, 690.
[78] L. Lu, Z. Huang, X. Li, X. Li, B. Cui, C. Yuan, L. Guo, P. Liu, Q. Dai. *Int. J. Biol. Macromol.* **2022**, *213*, 791.
[79] J. Deng, R. Bai, J. Zhao, G. Liu, Z. Zhang, W. You, W. Yu, X. Yan. *Angew. Chem., Int. Ed.* **2023**, *62*, e202309058.
[80] J. Zhang, Y. Hu, L. Zhang, J. Zhou, A. Lu. *Nano Micro Lett.* **2022**, *15*, 8,
[81] Q. Gao, F. Sun, Y. Li, L. Li, M. Liu, S. Wang, Y. Wang, T. Li, L. Liu, S. Feng, X. Wang, S. Agarwal, T. Zhang. *Nano Micro Lett.* **2023**, *15*, 139.
[82] B. Ding, P. Zeng, Z. Huang, L. Dai, T. Lan, H. Xu, Y. Pan, Y. Luo, Q. Yu, H.-M. Cheng, B. Liu. *Nat. Commun.* **2022**, *13*, 1212.
[83] S. Fu, X. Su, M. Li, S. Song, L. Wang, D. Wang, B. Z. Tang. *Adv. Sci.* **2020**, *7*, 2001909.
[84] Q. Liu, Y. He, Y. Fang, Y. Wu, G. Gong, X. Du, J. Guo. *Adv. NanoBiomed. Res.* **2023**, *3*, 2300046.
[85] S. Kim, A. U. Regitsky, J. Song, J. Ilavsky, G. H. McKinley, N. Holten-Andersen. *Nat. Commun.* **2021**, *12*, 667.
[86] J. Liu, X. Yang, M. Xu, H. Zhu, Y. Cheng, S. Li, T. Li, Y. Jiao, H. Song. *J. Mater. Chem. C* **2023**, *11*, 1184.
[87] M. Zhao, H. Zhuang, B. Li, M. Chen, X. Chen. *Adv. Mater.* **2023**, *35*, 2209944.
[88] J. Chen, X. Xu, M. Liu, Y. Li, D. Yu, Y. Lu, M. Xiong, I. Wyman, X. Xu, X. Wu. *Carbohydr. Polym.* **2021**, *264*, 117978.
[89] J. Liu, T. Luo, Y. Xue, L. Mao, P. J. Stang, M. Wang. *Angew. Chem.* **2021**, *133*, 5489.
[90] J. Kim, J. W. Kim, K. Keum, H. Lee, G. Jung, M. Park, Y. H. Lee, S. Kim, J. S. Ha. *Chem. Eng. J.* **2023**, *457*, 141278.
[91] F. Wang, C. Chen, D. Zhu, W. Li, J. Liu, J. Wang. *Int. J. Biol. Macromol.* **2023**, *253*, 126768.
[92] Y. Wang, X. Cao, J. Cheng, B. Yao, Y. Zhao, S. Wu, B. Ju, S. Zhang, X. He, W. Niu. *ACS Nano* **2021**, *15*, 3509.
[93] H. Wang, S. Wang, H. Su, K.-J. Chen, A. L. Armijo, W.-Y. Lin, Y. Wang, J. Sun, K. Kamei, J. Czernin, C. G. Radu, H.-R. Tseng. *Angew. Chem., Int. Ed.* **2009**, *48*, 4344.
[94] H. Meng, M. Xue, T. Xia, Y.-L. Zhao, F. Tamanoi, J. F. Stoddart, J. I. Zink, A. E. Nel. *J. Am. Chem. Soc.* **2010**, *132*, 12690.
[95] C.-Y. Quan, J.-X. Chen, H.-Y. Wang, C. Li, C. Chang, X.-Z. Zhang, R.-X. Zhuo. *ACS Nano* **2010**, *4*, 4211.
[96] G. Song, H. Sun, J. Chen, Z. Chen, B. Liu, Z. Liu, S. Cong, Z. Zhao. *Anal. Chem.* **2022**, *94*, 5048.
[97] X. Kang, M. Zhu. *Chem. Soc. Rev.* **2019**, *48*, 2422.
[98] A. Ghosh, S. Pandit, S. Kumar, D. Ganguly, S. Chattopadhyay, D. Pradhan, R. K. Das. *Chem. Eng. J.* **2023**, *475*, 146160.
[99] Y. Han, X. Wu, X. Zhang, C. Lu. *ACS Appl. Mater. Interfaces* **2017**, *9*, 20106.
[100] N. Yu, Y. Meng, R. Li, D. Mai, S. Shan, X. Wu, Y. Lin, A. Zhang. *J. Mater. Chem. A* **2024**, *12*, 12134.
[101] Y. Chen, Y. Shi, Y. Liang, H. Dong, F. Hao, A. Wang, Y. Zhu, X. Cui, Y. Yao. *ACS Appl. Energy Mater.* **2019**, *2*, 1608.
[102] P. Flouda, D. Bukharina, K. J. Pierce, A. V. Stryutsky, V. V. Shevchenko, V. V. Tsukruk. *ACS Appl. Mater. Interfaces* **2022**, *14*, 27028.
[103] S. Ghiassinejad, M. Ahmadi, E. van Ruymbeke, C.-A. Fustin. *Prog. Polym. Sci.* **2024**, *155*, 101854.
[104] S. Mena-Hernando, E. M. Pérez. *Chem. Soc. Rev.* **2019**, *48*, 5016.
[105] R. Bai, W. Wang, W. Gao, M. Yang, X. Zhang, C. Wang, Z. Fan, L. Yang, Z. Zhang, X. Yan. *Angew. Chem.* **2024**, *63*, e202410127.
[106] S. Ghiassinejad, A. Kumar Sharma, C.-A. Fustin, E. van Ruymbeke. *Chem. Mater.* **2024**, *36*, 8311.
[107] C. Gong, P. B. Balanda, H. W. Gibson. *Macromolecules* **1998**, *31*, 5278.
[108] G. De Bo, J. De Winter, P. Gerbaux, C.-A. Fustin. *Angew. Chem., Int. Ed.* **2011**, *50*, 9093.
[109] D. Aoki, S. Uchida, T. Takata. *ACS Macro Lett.* **2014**, *3*, 324.
[110] T. Higashi, T. Taharabaru, K. Motoyama. *Carbohydr. Polym.* **2024**, *337*, 122143.
[111] C. Przybylski, H. Ramoul, V. Bonnet, M. Abad, N. Jarroux. *Macromol. Chem. Phys.* **2019**, *220*, 1800502.
[112] C. Travelet, G. Schlatter, P. Hébraud, C. Brochon, A. Lapp, D. V. Anokhin, D. A. Ivanov, C. Gaillard, G. Hadziioannou. *Soft Matter* **2008**, *4*, 1855.
[113] S. Wang, Y. Chen, Y. Sun, Y. Qin, H. Zhang, X. Yu, Y. Liu. *Commun. Mater.* **2022**, *3*, 2.
[114] L. Chen, X. Sheng, G. Li, F. Huang. *Chem. Soc. Rev.* **2022**, *51*, 7046.
[115] W. Zhang, W. R. Dichtel, A. Z. Stieg, D. Benítez, J. K. Gimzewski, J. R. Heath, J. F. Stoddart. *Proc. Nat. Acad. Sci.* **2008**, *105*, 6514.
[116] B. D. Paulsen, S. Fabiano, J. Rivnay. *Annu. Rev. Mater. Res.* **2021**, *51*, 73.
[117] D. Meng, J. L. Yang, C. Xiao, R. Wang, X. Xing, O. Kocak, G. Aydin, I. Yavuz, S. Nuryyeva, L. Zhang, G. Liu, Z. Li, S. Yuan, Z.-K. Wang, W. Wei, Z. Wang, K. N. Houk, Y. Yang. *Proc. Nat. Acad. Sci.* **2020**, *117*, 20397.
[118] C. Musumeci, M. Vagin, E. Zeglio, L. Ouyang, R. Gabrielsson, O. Inganäs. *J. Mater. Chem. C* **2019**, *7*, 2987.
[119] H. Vazquez, R. Skouta, S. Schneebeli, M. Kamenetska, R. Breslow, L. Venkataraman, M. S. Hybertsen. *Nat. Nanotechnol.* **2012**, *7*, 663.
[120] S. B. Aziz, T. J. Woo, M. F. Z. Kadir, H. M. Ahmed. *J. Sci. Adv. Mater. Devices* **2018**, *3*, 1.
[121] Z. Chen, H. Liu, X. Lin, X. Mei, W. Lyu, Y. Liao. *Mater. Horiz.* **2023**, *10*, 3569.
[122] K. Hashimoto, T. Shiwaku, H. Aoki, H. Yokoyama, K. Mayumi, K. Ito. *Sci. Adv.* **2023**, *9*, eadi8505.
[123] W. Sun, Z. Xu, C. Qiao, B. Lv, L. Gai, X. Ji, H. Jiang, L. Liu. *Adv. Sci.* **2022**, *9*, 2201679.
[124] H. Kim, Y. Won, H. W. Song, Y. Kwon, M. Jun, J. H. Oh. *Adv. Sci.* **2024**, *11*, 2306191.
[125] N. Kamaya, K. Homma, Y. Yamakawa, M. Hirayama, R. Kanno, M. Yonemura, T. Kamiyama, Y. Kato, S. Hama, K. Kawamoto, A. Mitsui. *Nat. Mater.* **2011**, *10*, 682.
[126] J. Gao, C. Wang, D.-W. Han, D.-M. Shin. *Chem. Sci.* **2021**, *12*, 13248.
[127] K. M. Diederichsen, H. G. Buss, B. D. McCloskey. *Macromolecules* **2017**, *50*, 3831.
[128] R. Merkle, P. Gutbrod, P. Reinold, M. Katzmaier, R. Tkachov, J. Maier, S. Ludwigs. *Polymer* **2017**, *132*, 216.
[129] S. Varner, C. Balzer, Z.-G. Wang. *J. Phys. Chem. B* **2023**, *127*, 4328.
[130] A. Melianas, T. J. Quill, G. LeCroy, Y. Tuchman, H. Loo, S. T. Keene, A. Giovannitti, H. R. Lee, I. P. Maria, I. McCulloch, A. Salleo. *Sci. Adv.* **2020**, *6*, eabb2958.
[131] D. T. Hallinan, N. P. Balsara. *Annu. Rev. Mater. Res.* **2013**, *43*, 503.
[132] A. K. Verma, A. S. Thorat, J. K. Shah. *J. Ionic Liq.* **2024**, *4*, 100089.

[133] Z. Li, R. P. Misra, Y. Li, Y.-C. Yao, S. Zhao, Y. Zhang, Y. Chen, D. Blankschtein, A. Noy. *Nat. Nanotechnol.* **2023**, *18*, 177.
[134] Z. Shen, Q. Liang, Q. Chang, Y. Liu, Q. Zhang. *Adv. Mater.* **2024**, *36*, 2310365.
[135] J. Wang, Y. Chen, S. Tu, X. Cui, J. Chen, Y. Zhu. *J. Mater. Chem. C* **2024**, *12*, 14202.
[136] C. Wang, L. Dong, D. Peng, C. Pan. *Adv. Intell. Syst.* **2019**, *1*, 1900090.
[137] T. Dong, Y. Gu, T. Liu, M. Pecht. *Sens. Actuators, A* **2021**, *326*, 112720.
[138] M. W. Swift, J. W. Swift, Y. Qi. *Nat. Comput. Sci.* **2021**, *1*, 212.
[139] S. Fratini, M. Nikolka, A. Salleo, G. Schweicher, H. Sirringhaus. *Nat. Mater.* **2020**, *19*, 491.
[140] H. Chen, J. Fraser Stoddart. *Nat. Rev. Mater.* **2021**, *6*, 804.
[141] H. Chen, H. Zheng, C. Hu, K. Cai, Y. Jiao, L. Zhang, F. Jiang, I. Roy, Y. Qiu, D. Shen, Y. Feng, F. M. Alsubaie, H. Guo, W. Hong, J. F. Stoddart. *Matter* **2020**, *2*, 378.
[142] Z. Li, M. Smeu, A. Rives, V. Maraval, R. Chauvin, M. A. Ratner, E. Borguet. *Nat. Commun.* **2015**, *6*, 6321.
[143] H. Xia, G. Xu, X. Cao, C. Miao, H. Zhang, P. Chen, Y. Zhou, W. Zhang, Z. Sun. *Adv. Mater.* **2023**, *35*, 2301996.
[144] T. Zhou, Z. Qiao, M. Yang, K. Wu, N. Xin, J. Xiao, X. Liu, C. Wu, D. Wei, J. Sun. *Biosens. Bioelectron.* **2023**, *231*, 115288.
[145] Y. Liu, L. Wang, L. Zhao, Y. Zhang, Z.-T. Li, F. Huang. *Chem. Soc. Rev.* **2024**, *53*, 1592.
[146] T. Miyake, M. Rolandi. *J. Phys. Condens. Matter* **2016**, *28*, 023001.
[147] Y. Deng, E. Josberger, J. Jin, A. F. Roudsari, B. A. Helms, C. Zhong, M. P. Anantram, M. Rolandi. *Sci. Rep.* **2013**, *3*, 2481.
[148] J. H. Christie, I. M. Woodhead. *Text. Res. J.* **2002**, *72*, 273.
[149] G. Bardelmeyer. *Biopolymers: Original Res. Biomol.* **1973**, *12*, 2289.
[150] E. Murphy. *J. Colloid Interface Sci.* **1976**, *54*, 400.
[151] E. T. Nibbering, T. Elsaesser. *Chem. Rev.* **2004**, *104*, 1887.
[152] T. Kumagai, F. Hanke, S. Gawinkowski, J. Sharp, K. Kotsis, J. Waluk, M. Persson, L. Grill. *Phys. Rev. Lett.* **2013**, *111*, 246101.
[153] C. Zhou, X. Li, Z. Gong, C. Jia, Y. Lin, C. Gu, G. He, Y. Zhong, J. Yang, X. Guo. *Nat. Commun.* **2018**, *9*, 807.
[154] O. Butin, L. Pereyaslavets, G. Kamath, A. Illarionov, S. Sakipov, I. V. Kurnikov, E. Voronina, I. Ivahnenko, I. Leontyev, G. Nawrocki, M. Darkhovskiy, M. Olevanov, Y. K. Cherniavskyi, C. Lock, S. Greenslade, R. D. Kornberg, M. Levitt, B. Fain. *J. Chem. Theory Comput.* **2024**, *20*, 5215.
[155] J. Gao, X. Li, L. Xu, M. Yan, Q. Wang. *Int. J. Biol. Macromol.* **2024**, *280*, 135630.
[156] H. Ye, B. Wu, S. Sun, P. Wu. *Nat. Commun.* **2024**, *15*, 885.
[157] H. Xia, W. Zhou, X. Qu, W. Wang, X. Wang, R. Qiao, Y. Zhang, X. Wu, C. Yang, B. Ding, L. Y. Hu, Y. Ran, K. Yu, S. Hu, J. F. Li, H. M. Cheng, H. Qiu, J. Yin, W. Guo, L. Qiu. *Nat. Nanotechnol.* **2024**, *19*, 1316.
[158] Y. Liu, J. Zhang, X. Zhang, Y. Li, J. Wang. *ACS Appl. Mater. Interfaces* **2016**, *8*, 20352.
[159] M. Li, J. Qiao, C. Zhu, Y. Hu, K. Wu, S. Zeng, W. Yang, H. Zhang, Y. Wang, Y. Wu, R. Zang, X. Wang, J. Di, Q. Li. *ACS Appl. Electron. Mater.* **2021**, *3*, 944.
[160] Y. Zhao, B. Ashcroft, P. Zhang, H. Liu, S. Sen, W. Song, J. Im, B. Gyarfas, S. Manna, S. Biswas, C. Borges, S. Lindsay. *Nat. Nanotechnol.* **2014**, *9*, 466.
[161] S. Biswas, S. Sen, J. Im, S. Biswas, P. Krstic, B. Ashcroft, C. Borges, Y. Zhao, S. Lindsay, P. Zhang. *ACS Nano* **2016**, *10*, 11304.
[162] C. Wan, G. Chen, Y. Fu, M. Wang, N. Matsuhisa, S. Pan, L. Pan, H. Yang, Q. Wan, L. Zhu, X. Chen. *Adv. Mater.* **2018**, *30*, 1801291.
[163] Y. Lee, Y. Liu, D.-G. Seo, J. Y. Oh, Y. Kim, J. Li, J. Kang, J. Kim, J. Mun, A. M. Foudeh, Z. Bao, T.-W. Lee. *Nat. Biomed. Eng.* **2023**, *7*, 511.
[164] B. Coste, J. Mathur, M. Schmidt, T. J. Earley, S. Ranade, M. J. Petrus, A. E. Dubin, A. Patapoutian. *Science* **2010**, *330*, 55.
[165] S. Chen, Z. Zhou, K. Hou, X. Wu, Q. He, C. G. Tang, T. Li, X. Zhang, J. Jie, Z. Gao, N. Mathews, W. L. Leong. *Nat. Commun.* **2024**, *15*, 7056.
[166] B. U. Ye, B.-J. Kim, J. Ryu, J. Y. Lee, J. M. Baik, K. Hong. *Nanoscale* **2015**, *7*, 16189.
[167] H. L. Wang, Z. H. Guo, G. Zhu, X. Pu, Z. L. Wang. *ACS Nano* **2021**, *15*, 7513.
[168] W. Xu, L.-B. Huang, M.-C. Wong, L. Chen, G. Bai, J. Hao. *Adv. Energy Mater.* **2017**, *7*, 1601529.
[169] K.-H. Ke, C.-K. Chung. *Small* **2020**, *16*, 2001209.
[170] Y. Zhang, J. Yang, X. Hou, G. Li, L. Wang, N. Bai, M. Cai, L. Zhao, Y. Wang, J. Zhang, K. Chen, X. Wu, C. Yang, Y. Dai, Z. Zhang, C. F. Guo. *Nat. Commun.* **2022**, *13*, 1317.
[171] S. Zhou, T.-H. Han, L. Ding, E. Ru, C. Zhang, Y.-J. Zhang, C.-X. Yi, T.-S. Sun, Z.-Y. Luo, Y. Liu. *Adv. Funct. Mater.* **2024**, *34*, 2313012.
[172] M. Arefian, M. Hojjati, I. Tajzad, A. Mokhtarzade, M. Mazhar,A. Jamavari. *J. Composit. Compounds* **2020**, *2*, 69.
[173] M. Qin, W. Yuan, X. Zhang, Y. Cheng, M. Xu, Y. Wei, W. Chen, D. Huang. *Colloids Surf. B* **2022**, *214*, 112482.
[174] D. Da Silva, M. Kaduri, M. Poley, O. Adir, N. Krinsky, J. Shainsky-Roitman, A. Schroeder. *Chem. Eng. J.* **2018**, *340*, 9.
[175] S. Stříteský, A. Marková, J. Víteček, E. Šafaříková, M. Hrabal, L. Kubáč, L. Kubala, M. Weiter, M. Vala. *J. Biomed. Mater. Res. Part A* **2018**, *106*, 1121.
[176] C. Wang, J. Zhang, H. Chen, Z. Wang, C. Huang, Y. Tan. *J. Mater. Chem. C* **2022**, *10*, 8077.
[177] V. Amoli, J. S. Kim, S. Y. Kim, J. Koo, Y. S. Chung, H. Choi, D. H. Kim. *Adv. Funct. Mater.* **2020**, *30*, 1904532.
[178] M. Dong, B. Shi, D. Liu, J.-H. Liu, D. Zhao, Z.-H. Yu, X.-Q. Shen, J.-M. Gan, B.-l. Shi, Y. Qiu, C.-C. Wang, Z.-Z. Zhu, Q.-D. Shen. *ACS Nano* **2020**, *14*, 16565.
[179] Q. Liu, G. Nian, C. Yang, S. Qu, Z. Suo. *Nat. Commun.* **2018**, *9*, 846.
[180] K. Kang, S. Ye, C. Jeong, J. Jeong, Y. Ye, J.-Y. Jeong, Y.-J. Kim, S. Lim, T. H. Kim, K. Y. Kim, J. U. Kim, G. I. Kim, D. H. Chun, K. Kim, J. Park, J.-H. Hong, B. Park, K. Kim, S. Jung, K. Baek, D. Cho, J. Yoo, K. Lee, H. Cheng, B.-W. Min, H. J. Kim, H. Jeon, H. Yi, T. Kim, K. J. Yu, Y. Jung. *Nat. Commun.* **2024**, *15*, 10.
[181] Z. Tan, L. Xiao, J. Ma, K. Shi, J. Liu, F. Feng, P. Xie, Y. Dai, Q. Yuan, W. Wu, L. Rong, L. He. *Sci. Adv.* **2024**, *10*, eado9120.
[182] Y. Huang, J. Zhou, P. Ke, X. Guo, C. K. Yiu, K. Yao, S. Cai, D. Li, Y. Zhou, J. Li, T. H. Wong, Y. Liu, L. Li, Y. Gao, X. Huang, H. Li, J. Li, B. Zhang, Z. Chen, H. Zheng, X. Yang, H. Gao, Z. Zhao, X. Guo, E. Song, H. Wu, Z. Wang, Z. Xie, K. Zhu, X. Yu. *Nat. Electron.* **2023**, *6*, 1020.
[183] T. Li, Y. Yan, C. Yu, J. An, Y. Wang, G. Chen. *Rob. Comput. Integr. Manuf.* **2024**, *90*, 102792.
[184] X. Guo, Z. Sun, Y. Zhu, C. Lee. *Adv. Mater.* **2024**, *36*, 2406778.
[185] J. Wang, R. Chen, D. Ji, W. Xu, W. Zhang, C. Zhang, W. Zhou, T. Luo. *Small* **2024**, *20*, 2307800.
[186] D. Liu, X. Tian, J. Bai, S. Wang, S. Dai, Y. Wang, Z. Wang, S. Zhang. *Nat. Electron.* **2024**, *7*, 1176.
[187] L. Zhang, L. Chen, S. Wang, S. Wang, D. Wang, L. Yu, X. Xu, H. Liu, C. Chen. *Nat. Commun.* **2024**, *15*, 3859.
[188] N. Bosnjak, M. N. Silberstein. *Science* **2021**, *374*, 150.
[189] Z. Wang, X. Zheng, T. Ouchi, T. B. Kouznetsova, H. K. Beech, S. Av-Ron, T. Matsuda, B. H. Bowser, S. Wang, J. A. Johnson, J. A. Kalow, B. D. Olsen, J. P. Gong, M. Rubinstein, S. L. Craig. *Science* **2021**, *374*, 193.

Mingqi Ding is currently a Ph.D. student at the Department of Materials Science and Engineering, City University of Hong Kong. He received his B.S. degree from Harbin Engineering University in 2020 and his M.S. degree from Sichuan University in 2023, respectively. His research interests mainly focus on fabricating flexible devices, including ionic hydrogels, artificial mechanoreceptors, and novel hydrogel semiconductors.

Pengshan Xie is a postdoctoral researcher at the Department of Materials Science and Engineering, City University of Hong Kong. He received his B.S. and M.S. degrees from Central South University in 2017 and 2020, respectively. He then received his Ph.D. degree from the City University of Hong Kong in 2024. His research interests mainly focus on the fabrication of nanomaterial devices, including III-V semiconductor nanowires, novel neuromorphic electronics, and field-effect transistors, etc.

Johnny C. Ho is a Professor of Materials Science and Engineering at the City University of Hong Kong. He received his B.S. degree in Chemical Engineering and his M.S. and Ph.D. degrees in Materials Science and Engineering from the University of California, Berkeley, in 2002, 2005, and 2009, respectively. From 2009–2010, he was a Postdoctoral Research Fellow in the Nanoscale Synthesis and Characterization Group at Lawrence Livermore National Laboratory. His research interests focus on the synthesis, characterization, integration, and device applications of nanoscale materials for various technological applications, including nanoelectronics, sensors, and energy harvesting.